Mechanics of Advanced Materials and Structures

ISSN: (Print) (Online) Journal homepage: www.tandfonline.com/journals/umcm20

Modeling and analysis of Double-Double composite structures integrating piezoelectric materials

B. D. Lupu & M. A. R. Loja

To cite this article: B. D. Lupu & M. A. R. Loja (18 Apr 2024): Modeling and analysis of Double-Double composite structures integrating piezoelectric materials, Mechanics of Advanced Materials and Structures, DOI: 10.1080/15376494.2024.2338910

To link to this article: https://doi.org/10.1080/15376494.2024.2338910

MECHANICS OF ADVANCED MATERIALS AND STRUCTURES
https://doi.org/10.1080/15376494.2024.2338910

Taylor & Francis
Taylor & Francis Group

ORIGINAL ARTICLE

Modeling and analysis of Double-Double composite structures integrating piezoelectric materials

B. D. Lupu[a] and M. A. R. Loja[a,b]

[a]CIMOSM, ISEL, IPL–Centro de Investigação em Modelação e Otimização de Sistemas Multifuncionais, Instituto Superior de Engenharia de Lisboa, Lisbon, Portugal; [b]IDMEC, IST–Instituto Superior Técnico, Universidade de Lisboa, Lisbon, Portugal

ABSTRACT

Multifunctional materials and structures are increasingly important for innovative structural solutions. This work aims to model such structures constituted by Double-Double composites and piezoelectric materials. Besides the homogenization trend of these laminates as the number of the replicating sub-laminates grows, other features include simple ply drop placement, and card sliding to potentially save weight. To control the mechanical response, piezoelectrics along with several types of stacking were considered. The first-order shear deformation theory implemented *via* the finite element method was used to assess the model, and a set of verification and parametric studies was developed, resulting in a good performance confirmation.

Nomenclature: AFC: active fiber composites; $BaTiO_3$: piezoceramic barium titanate; BB: building-block; CFRP: carbon fiber-reinforced polymer; DD: Double-Double; EBCs: electric boundary conditions; FDM: fused deposition modeling; FSDT: first-order shear deformation theory; MBCs: mechanical boundary conditions; MFC: macro-fiber composites; PVDF: polymer polyvinylidene fluoride; PZT: lead zirconate titanate; SDL: doubly sinusoidal load; UDL: uniformly distributed loads

ARTICLE HISTORY
Received 15 December 2023
Accepted 1 April 2024

KEYWORDS
Adaptive structures; piezoelectric materials; Double-Double composites; tapered laminates; finite element modeling

1. Introduction

Adaptive composite structures are in general achieved *via* a relevant engineering combination of passive and active materials that link the advantages of mechanical strength and stiffness/weight ratio of the composites with the active capabilities of the so-called smart materials. In the last decades, this subject has undergone increasing growth in terms of research and development, and therefore, the literature found in these fields is very significant [1]. These developments led to diverse applications, such as vibration damping, shape control, noise and acoustic control, energy harvesting, and health monitoring, among many others. The integration of piezoelectric sensors and actuators, whether embedded or surface-mounted, into composite structures, referred to as hybrid laminates, stands as an important component in the advancement of smart structures [2]. The piezoelectricity was discovered by Jacques and Pierre Curie in 1880 [3] when they realized that this electromechanical phenomenon coupled the mechanical and electrical fields. It was found that piezoelectric materials generated an electric charge when subjected to a mechanical deformation, constituting the known direct piezoelectric effect. Conversely, mechanical stress or strain is produced by an applied electric field, this being called the converse piezoelectric effect [4]. Common types of materials that exhibit piezoelectricity are piezoceramic barium titanate ($BaTiO_3$), lead zirconate titanate (PZT), and polymer polyvinylidene fluoride (PVDF) [5]. Also, well-known are the piezo-fiber-based composites, active fiber composites (AFC), and macro-fiber composites (MFC) because of the integration of the piezoceramic fibrous phase into an epoxy matrix phase [6]. Some recent comprehensive reviews on state-of-the-art about piezoelectric energy harvesting were presented by Sezer and Koç [3], Safaei et al. [7], and Aabid et al. [8]. For the proper implementation of laminates incorporating piezoelectric materials, it is crucial to develop appropriate analysis theories to accurately model and predict their structural behavior [9]. Over the years several approaches have been presented including analytical and numerical-based piezoelasticity solutions considering various theories and hypotheses. Therefore, some important reviews related to the modeling of smart piezoelectric composite laminates were presented by Saravanos and Heyliger [10], Benjeddou [11], Kapuria et al. [2], and—more recently, by Zhang et al. [6]—where relevant contributions to this subject were presented. Additionally, Carrera conducted a pertinent historical review [12] on Zig-Zag theories and more recently, a review of structural theories by Carrera et al. [13].

In this context and focusing on relevant research topics, such as the design of energy harvesting systems for illustrative purposes, it is worth referring to the works of Chattaraj

CONTACT B. D. Lupu bogdan.lupu.sci@gmail.com CIMOSM, ISEL, IPL–Centro de Investigação em Modelação e Otimização de Sistemas Multifuncionais, Instituto Superior de Engenharia de Lisboa, R. Conselheiro Emídio Navarro 1, Lisbon, 1959-007, Portugal; M. A. R. Loja amelia.loja@isel.pt CIMOSM, ISEL, IPL–Centro de Investigação em Modelação e Otimização de Sistemas Multifuncionais, Instituto Superior de Engenharia de Lisboa, R. Conselheiro Emídio Navarro 1, Lisbon, 1959-007, Portugal.

and Ganguli [14], Raju et al. [15], Anilkumar et al. [16], and due to Kurt et al. [17], among others.

Chattaraj and Ganguli [14] investigated the performance improvement of a piezo-bimorph actuator by tailoring its geometry. Those authors presented analytically and *via* finite element results that a piezo-bimorph actuator with a tapered surface provides superior performance for out-of-plane bending when compared to a rectangular surface while having equal mass and equal primary capacitance. Two different structurally tailored cantilever-based piezoelectric energy harvesters were proposed and investigated by Raju et al. [15] to improve the harvested power. Anilkumar et al. [16] presented a study where tailoring options in variable stiffness laminates were exploited to obtain low snap-through and snap-back voltages while enabling high out-of-plane displacements using microfiber composite actuators. More recently Kurt et al. [17] studied the mechanical energy transfer between the source structure and active material in piezoelectric energy harvesters. Those authors proposed tailoring the stiffness of the beam to off-the-shelf piezo-composites and have validated this approach through numerical models and experiments. Moreover, a general discussion on plates and shells for smart structures can be found in Carrera et al. [18].

For many years, the industry has studied and widely applied layers comprising four main orientations, the so-called "Legacy Quad" or just "QUAD": 0, 90, +45, and −45° [19–22]. As a result of its use, several empirical rules or guidelines have been developed – commonly known as stacking rules—and applied, such as the 10% (sometimes 8%) rule, the balance requirement of ± plies, and one of the most-important, the symmetry requirement [22]. Although these rules have proved their effectiveness, they also contribute to non-optimal laminate stackings, resulting in unnecessarily heavy carbon fiber reinforced polymer (CFRP) components and presenting significant challenges in the context of laminate optimization [20,22].

The optimal design of laminates is a very important field that has drawn the attention of many researchers in the last decades. This is well illustrated by the works of Vannucci [23] and Vincenti et al. [24]. Vannucci [23] proposed a general approach to the optimal design of smart laminates, acted by piezoelectric patches. The original, minimizing problem with at least one equality constraint, is split into two sequential optimization problems, the first one being almost trivial and the second one being unconstrained or eventually submitted to only inequality constraints, so receiving a suitable numerical solution by a meta heuristic, in this case, an adaptive PSO algorithm. Another work on the development of a general approach to the optimal design of composite laminates where elastic symmetries can also be explicitly expressed as criteria of the optimization process is proposed by Vincenti et al. [24].

In the most recent years, one may refer among others, to the investigation carried out by Montemurro and Catapano [25] focused on the optimum design of variable angle tow composites by using a generalization of a multiscale two-level optimization based on a hybrid optimization tool (genetic- and gradient-based algorithms). The authors used the polar formalism to describe the laminate behavior, and iso geometric surfaces to describe the spatial variation of the stiffness properties. Montemurro et al. [26] addressed the problem of minimizing the weight design of a composite multilayer plate subject to a diversity of constraints, namely mechanical, geometrical, and technological ones. To face this problem, the authors considered a multiscale two-level optimization approach based on polar formalism to describe the macroscopic behavior of the composites and on a special genetic algorithm to perform composite calculations.

More recently, Catapano and Montemurro [27] exploited a multiscale two-level optimization strategy to find the best solution for the strength of variable angle-tow composites subject to mechanical and manufacturing constraints. In the first phase of this strategy, the laminate strength is described through a laminate-level failure criterion based on tensor invariants and considering the use of the first-order shear deformation theory. The stacking design phase makes use of quasi-trivial solutions and integrates a check on the first-ply failure to ensure the integrity of the whole laminate. A new strategy to deal with blending requirements in the composite structures design was developed by Scardaoni et al. [28]. The first step of this strategy consists of deriving the analytical expressions of blending constraints, in the polar parameters space, and subsequently, through a dedicated numerical strategy, it is considered the recovery of blended stacking sequences. This approach was implemented in the framework of a multiscale two-level optimization strategy.

Double-Double (DD) laminates were introduced by Tsai [20] as a different approach to laminates. This family is characterized by a sub-laminate main block (Building Block, BB) and a total repetition parameter "*rT*." The block is made up of a stack of four layers, $[\pm\Phi/\pm\psi]$ with angles ranging from 0 to 90° with the better-performing block being: $[\Phi/-\psi/-\Phi/\psi]rT$—known as "Staggered 1." According to the author, there are several advantages to this approach, which include a homogenization trend, tapering to save weight, ply drop placement to improve quality, and the card sliding method to simplify ply stacking and save weight. These characteristics reflect better tailoring and cheaper manufacturing, which opens potential optimization opportunities for stiffness, strength, and buckling improvement, among others [29]. However, it is important to note that the solutions obtained by considering those building blocks, although being able to improve some performance aspects or features, do not mean to be exhaustive, not guaranteeing optimal solutions. DD laminates are a sub-set of the most general family of quasi-trivial (QT) stacking sequences, which although orthotropic in membrane are anisotropic in bending. In this context it is pertinent to mention the work due of Garulli et al. [30], where new properties of QT layups were derived, allowing to obtain QT sequences by superposing any number of QT elementary stacks and enabling a relevant tool in the design and optimization of composites laminates. It is also important to quote here the work developed by Scardaoni et al. [28] and by Scardaoni and Montemurro [31], where a laminates' blending

construction methodology was presented, regardless of the orientation value and the position of the dropped plies.

The invariant-based approach proposed by Tsai and Melo [32] to describe the elastic properties and failure of carbon fiber-reinforced composite laminates and other publications regarding this approach paved the way for the DD concept. Although this approach does not allow to characterize the elastic symmetries of the tensors involved in different laminates theories it has been considered in subsequent DD-related works, possibly due to its implementation simplicity characteristics. It should however be noted that the polar method introduced by Verchery [33] and the subsequent works due by Vannucci and Verchery [34], Vannucci [35], and Montemurro [36] allow for mathematically rigorous approaches while extending the polar formalism to more refined theories.

The trace-based approach presented in works, such as [37–39], presented the use of the trace-based theory as a stress–strain relation to set up scaling among various materials/laminates and as a direct laminate sizing method based on the trace and unit circle failure criteria proposed in Ref. [40]. The theory of the master ply concept for invariant-based stiffness of composites was validated by Ha and Cimini Jr. [41] concerning carbon/epoxy and aramid/epoxy material systems and later by Guedes [42], focusing on aramid and glass-reinforced polymer composites. Micromechanical models have been developed concerning the invariant-based approach as presented by Arteiro et al. [43], confirming the empirical observations from Tsai and Melo [32] and also the applicability of the Master Ply based on the median values of several CFRPs. Also, Arteiro et al. [44] view the invariant-based approach and Tsai's modulus. Millen et al. [45], extended the application of invariants to woven and hybrid composites providing appropriate validation for their use in design. Vignoli et al. [46], presented a comparison between traditional micromechanical models and the Tsai trace-based approach, illustrating the reduction in the expense of composite design with a reliable estimation. More recently, Jia et al. [47] focused on the development of trace-based invariant theory introducing a novel mathematical proof for expressing thickness-normalized stiffness and extending this method to apply third-order transverse shear deformation theory for stiffness analysis in hybrid laminates. Vignoli et al. [48], validated Tsai's modulus approach for determining lamina effective properties in CFRP by comparing it with two micromechanical models, demonstrating that the difference is $<15\%$ across various laminae' elastic properties, thereby offering a theoretical justification for Tsai's modulus. Patel and Desai [49], performed an experimental analysis of four Fused Deposition Modeling (FDM) materials, employing invariant-based and master ply approaches to predict elastic properties particularly emphasizing its effectiveness for unidirectional FDM materials. Their study showed the potential to reduce experimental tests, highlighting its unique material property application for predicting elastic modulus. More details on the invariant-based approach can be found extensively in Refs. [50,51].

The presentation of the Double-Double approach was made by Tsai et al. [52], formally by Tsai [20] and later in a comprehensive format [53]. Vermes et al. [21], discussed the idea, advantages, and validity of both Tsai's modulus and the DD theories. Also, Vermes et al. [19], showed that layup homogenization is a powerful method to mitigate the warpage of asymmetric layups and that the laminate design and manufacturing processes can be simpler and less prone to error using the DD approach with significant weight savings. Kappel [22], presented a closed strategy for finding the better DD laminates for given load sets employing an optimization scheme in combination with the Nettles circle failure envelope. He also showed how the detrimental asymmetry effects, such as warpage and bending–twist coupling, diminish proportionally with $1/r$ and $1/r^2$. More recently, Zhang et al. [54] used machine learning to rapidly and accurately predict DD CFRP simulation results under various loading conditions focusing on achieving a significant reduction in simulation time using data-driven algorithms while maintaining high accuracy and with potential extensions to more complex cases. Wang et al. [29], addressed topology optimization for DD composite laminates, specifically focusing on stress control by proposing a nested p-norm method that integrates the Tsai–Hill failure criteria indexes of different elements in different layers into one design response. Vescovini et al. [55] analyzed the post-buckling behavior and collapse of DD composite single stringer specimens by employing numerical simulations validated by experimental tests. Their study highlighted the tapering caused by the card-sliding technique and the potential benefits of DD for designing composite structures less susceptible to delamination and intra-laminar failure.

DD stacks may not be the best, optimal solution for problems that require lightness, membrane orthotropy, bending orthotropy, and membrane/bending uncoupling when compared to QT stacks, with which it is possible to meet the homogeneity and uncoupling requirements with a smaller number of plies. However, although being a non-optimal sub-class of this more general family, it is worth investigating the performance of these laminates, being thus the main objective of the present study.

To the best of the author's knowledge, no studies or research within the multi-field problems, considering DD laminates integrating piezoelectric patches/layers have been presented so far. In this work, the objective is to model, analyze, and predict the mechanical behavior of such beam and plate-type hybrid composite structures, considering the DD conversion and card-sliding technique in parallel to the sensing and actuation capabilities brought by the piezoelectric materials.

The remainder part of this work is organized as follows: Section 2 describes the methodology adopted in the present study focusing on the materials characterization and the procedure/method used for performing the analyses; Section 3 presents and discusses the results achieved, organized in terms of verification studies and other case studies. Finally, in Section 4 some conclusions are drawn based on the results achieved.

2. Methodology

2.1. Material modeling, displacement field, and constitutive relations

For a generic composite laminate, if one considers it to be valid assuming that the layers are in a plane state of stress, it is possible to use the first-order shear deformation theory (FSDT) [1,50,56] to model and analyze that laminate. Therefore, the constitutive relation for a generic layer k, made of an orthotropic piezoelectric material, under such conditions is presented in Eq. (1):

$$\begin{Bmatrix}\sigma_{xx}\\ \sigma_{yy}\\ \tau_{xy}\\ \tau_{xz}\\ \tau_{yz}\end{Bmatrix}^k = \begin{bmatrix}\overline{Q}_{11} & \overline{Q}_{12} & \overline{Q}_{16} & 0 & 0\\ \overline{Q}_{12} & \overline{Q}_{22} & \overline{Q}_{26} & 0 & 0\\ \overline{Q}_{16} & \overline{Q}_{26} & \overline{Q}_{66} & 0 & 0\\ 0 & 0 & 0 & \overline{Q}_{44} & \overline{Q}_{45}\\ 0 & 0 & 0 & \overline{Q}_{45} & \overline{Q}_{55}\end{bmatrix}^k \begin{Bmatrix}\varepsilon_{xx}\\ \varepsilon_{yy}\\ \gamma_{xy}\\ \gamma_{xz}\\ \gamma_{yz}\end{Bmatrix} - \begin{bmatrix}0 & 0 & \overline{e}_{31}\\ 0 & 0 & \overline{e}_{32}\\ 0 & 0 & \overline{e}_{36}\\ \overline{e}_{14} & \overline{e}_{24} & 0\\ \overline{e}_{15} & \overline{e}_{25} & 0\end{bmatrix}^k \begin{Bmatrix}\mathrm{E}_x\\ \mathrm{E}_y\\ \mathrm{E}_z\end{Bmatrix}$$
$$\begin{Bmatrix}\mathcal{D}_x\\ \mathcal{D}_y\\ \mathcal{D}_z\end{Bmatrix}^k = \begin{bmatrix}0 & 0 & 0 & \overline{e}_{14} & \overline{e}_{15}\\ 0 & 0 & 0 & \overline{e}_{24} & \overline{e}_{25}\\ \overline{e}_{31} & \overline{e}_{32} & \overline{e}_{36} & 0 & 0\end{bmatrix}^k \begin{Bmatrix}\varepsilon_{xx}\\ \varepsilon_{yy}\\ \gamma_{xy}\\ \gamma_{xz}\\ \gamma_{yz}\end{Bmatrix} + \begin{bmatrix}\overline{\epsilon}_{11} & \overline{\epsilon}_{12} & 0\\ \overline{\epsilon}_{12} & \overline{\epsilon}_{22} & 0\\ 0 & 0 & \overline{\epsilon}_{33}\end{bmatrix}^k \begin{Bmatrix}\mathrm{E}_x\\ \mathrm{E}_y\\ \mathrm{E}_z\end{Bmatrix} \tag{1}$$

where the vector of the stress components $\{\sigma\}$ and the vector of the electric displacements $\{\mathcal{D}\}$, are functions of the transformed plane stress-reduced elastic stiffness coefficients $\overline{Q}_{ij}$, electric permittivities $\overline{\epsilon}_{ij}$, and piezoelectric coefficients $\overline{e}_{ij}$. These coefficients can be described as follows:

$$\begin{aligned}
\overline{Q}_{11} &= \tilde{Q}_{11}\cos^4\theta + 2\left(\tilde{Q}_{12} + 2\tilde{Q}_{66}\right)\sin^2\theta\cos^2\theta + \tilde{Q}_{22}\sin^4\theta\\
\overline{Q}_{12} &= \left(\tilde{Q}_{11} + \tilde{Q}_{22} - 4\tilde{Q}_{66}\right)\sin^2\theta\cos^2\theta + \tilde{Q}_{12}(\cos^4\theta + \sin^4\theta)\\
\overline{Q}_{22} &= \tilde{Q}_{11}\sin^4\theta + 2\left(\tilde{Q}_{12} + 2\tilde{Q}_{66}\right)\sin^2\theta\cos^2\theta + \tilde{Q}_{22}\cos^4\theta\\
\overline{Q}_{16} &= \left(\tilde{Q}_{11} - \tilde{Q}_{12} - 2\tilde{Q}_{66}\right)\sin\theta\cos^3\theta + \left(\tilde{Q}_{12} - \tilde{Q}_{22} + 2\tilde{Q}_{66}\right)\sin^3\theta\cos\theta\\
\overline{Q}_{26} &= \left(\tilde{Q}_{11} - \tilde{Q}_{12} - 2\tilde{Q}_{66}\right)\sin^3\theta\cos\theta + \left(\tilde{Q}_{12} - \tilde{Q}_{22} + 2\tilde{Q}_{66}\right)\sin\theta\cos^3\theta\\
\overline{Q}_{66} &= \left(\tilde{Q}_{11} + \tilde{Q}_{22} - 2\tilde{Q}_{12} - 2\tilde{Q}_{66}\right)\sin^2\theta\cos^2\theta + \tilde{Q}_{66}(\sin^4\theta + \cos^4\theta)\\
\overline{Q}_{44} &= \tilde{Q}_{44}\cos^2\theta + \tilde{Q}_{55}\sin^2\theta\\
\overline{Q}_{45} &= \left(\tilde{Q}_{55} - \tilde{Q}_{44}\right)\cos\theta\sin\theta\\
\overline{Q}_{55} &= \tilde{Q}_{55}\cos^2\theta + \tilde{Q}_{44}\sin^2\theta
\end{aligned} \tag{2}$$

where $\tilde{Q}_{ij}$ denotes the plane stress-reduced elastic coefficients as presented in Eq. (3):

$$\begin{aligned}
&\tilde{Q}_{11} = Q_{11} - \frac{Q_{13}^2}{Q_{33}};\ \tilde{Q}_{12} = Q_{12} - \frac{Q_{13}Q_{23}}{Q_{33}};\ \tilde{Q}_{22} = Q_{22} - \frac{Q_{23}^2}{Q_{33}}\\
&\tilde{Q}_{44} = Q_{44};\ \tilde{Q}_{55} = Q_{55};\ \tilde{Q}_{66} = Q_{66}
\end{aligned} \tag{3}$$

Although the phenomenon of piezoelectricity has a non-linear behavior [1,57–59] it can be considered linear for small variations in the electric field [1,4,57,60] and is therefore defined by linear coefficients. It should be noted that piezoelectric coupling components can be presented in a strain-charge format, $d_{ij}(x,y,z)$ or stress-charge, $e_{ij}(x,y,z)$. The matrix of these latter transformed plane stress-reduced piezoelectric coefficients for a given k-th piezoelectric layer is given as [4,57]:

$$[\overline{e}]^k = \begin{bmatrix}0 & 0 & 0 & \overline{e}_{14} & \overline{e}_{15}\\ 0 & 0 & 0 & \overline{e}_{24} & \overline{e}_{25}\\ \overline{e}_{31} & \overline{e}_{32} & \overline{e}_{36} & 0 & 0\end{bmatrix}^k \tag{4}$$

where these coefficients can be described as follows:

$$\begin{aligned}
\overline{e}_{31} &= \tilde{e}_{31}\cos^2\theta + \tilde{e}_{32}\sin^2\theta\\
\overline{e}_{32} &= \tilde{e}_{31}\sin^2\theta + \tilde{e}_{32}\cos^2\theta\\
\overline{e}_{36} &= (\tilde{e}_{31} - \tilde{e}_{32})\sin\theta\cos\theta\\
\overline{e}_{15} &= \tilde{e}_{15}\cos^2\theta + \tilde{e}_{24}\sin^2\theta\\
\overline{e}_{25} &= (\tilde{e}_{15} - \tilde{e}_{24})\sin\theta\cos\theta\\
\overline{e}_{14} &= (\tilde{e}_{15} - \tilde{e}_{24})\sin\theta\cos\theta\\
\overline{e}_{24} &= \tilde{e}_{24}\cos^2\theta + \tilde{e}_{15}\sin^2\theta
\end{aligned} \tag{5}$$

where $\tilde{e}_{ij}$ denotes the plane stress-reduced piezoelectric coefficients as presented in Eq. (6):

$$\begin{aligned}
&\tilde{e}_{31} = e_{31} - \frac{Q_{13}e_{33}}{Q_{33}};\ \tilde{e}_{32} = e_{32} - \frac{Q_{23}e_{33}}{Q_{33}};\\
&\tilde{e}_{15} = e_{15};\ \tilde{e}_{24} = e_{24};\ \tilde{e}_{36} = e_{36}
\end{aligned} \tag{6}$$

Similarly, the coefficients relating to the polarization of the piezoelectric material $\overline{\epsilon}_{ij}$ are presented in the permittivity matrix $[\overline{\epsilon}]^k$ defined in Eq. (7):

$$[\overline{\epsilon}]^k = \begin{bmatrix}\overline{\epsilon}_{11} & \overline{\epsilon}_{12} & 0\\ \overline{\epsilon}_{12} & \overline{\epsilon}_{22} & 0\\ 0 & 0 & \overline{\epsilon}_{33}\end{bmatrix}^k \tag{7}$$

where $\overline{\epsilon}_{ij}$ denotes the transformed plane stress-reduced permittivity coefficients, described as:

$$\begin{aligned}
\overline{\epsilon}_{11} &= \tilde{\epsilon}_{11}\cos^2\theta + \tilde{\epsilon}_{22}\sin^2\theta\\
\overline{\epsilon}_{22} &= \tilde{\epsilon}_{11}\sin^2\theta + \tilde{\epsilon}_{22}\cos^2\theta\\
\overline{\epsilon}_{33} &= \tilde{\epsilon}_{33}\\
\overline{\epsilon}_{12} &= (\tilde{\epsilon}_{11} - \tilde{\epsilon}_{22})\sin\theta\cos\theta
\end{aligned} \tag{8}$$

where $\tilde{\epsilon}_{ij}$ denotes the plane stress-reduced permittivity coefficients as presented in Eq. (9):

$$\tilde{\epsilon}_{11} = \epsilon_{11};\ \tilde{\epsilon}_{22} = \epsilon_{22};\ \tilde{\epsilon}_{33} = \epsilon_{33} + \frac{e_{33}^2}{Q_{33}} \tag{9}$$

Note that only the polarization in the thickness direction (z) is considered, similar to Ref. [61]. It is also worth noting that the piezoelectric shear contributions are not considered, i.e. e_{ij} with $ij = \{14, 24, 15, 25\}$ are always zero. Then, the electric field E_z is defined as follows:

$$\mathrm{E}_z = -\frac{\partial\phi}{\partial z} = -\frac{\phi}{h_p} \tag{10}$$

where ϕ denotes the electric potential and h_p the thickness of the respective layer. Considering the elastic behavior of the laminate, it is possible to define the extensional stiffness matrix [A], the bending-extensional coupling stiffness matrix [B], and the bending stiffness matrix [D] as follows [62]:

$$\{A_{ij}, B_{ij}, D_{ij}\} = \sum_{k=1}^{N_c} \left\{ \int_{z_k}^{z_{k+1}} \overline{Q}_{ij}^{k}(1, z, z^2)dz \right\} \tag{11}$$

It should be noted that when the piezoelectric effect is present, the expressions will contain the respective forces generated as shown in Eq. (1).

Several theories attempt to model the behavior of structures by proposing a diversity of displacement fields. According to Ref. [62], Equivalent Single-Layer (ESL) theories reduce the 3D elasticity problem to 2D and describe the displacement field as a linear combination between the unknown functions and the thickness coordinate. The first-order shear deformation theory, implemented in the present study, is part of the 2D-ESL set of theories. Its simplicity and low computational cost make this approach very attractive, obtaining accurate results for thin and moderately thick structures [13]. This theory considers the existence of transverse shear deformations and corresponding transverse stresses, although with a constant through-thickness profile and inextensibility in the thickness direction ($\varepsilon_{zz} = 0$), leading to a transverse displacement w independent of the z coordinate [62]. This is evidenced by the respective displacement field, described as follows:

$$\begin{aligned} u(x, y, z) &= u^0(x, y) + z \cdot \theta_x^0(x, y) \\ v(x, y, z) &= v^0(x, y) + z \cdot \theta_y^0(x, y) \\ w(x, y, z) &= w^0(x, y) \end{aligned} \tag{12}$$

where, u, v, and w represent the displacements at a generic point with coordinates (x, y, z); u^0, v^0, and w^0 represent the displacements at a generic point (x, y) on the plate's middle surface; θ_x^0 and θ_y^0 represent the rotations of the transverse normal around oX and oY. Then, considering the elasticity theory for small deformations and considering their respective kinematic relations, the displacement field is given as presented in Eq. (13):

$$\begin{aligned} \varepsilon_{xx} &= \frac{\partial u}{\partial x} = \frac{\partial u^0}{\partial x} + z\frac{\partial \theta_x^0}{\partial x} \\ \varepsilon_{yy} &= \frac{\partial v}{\partial y} = \frac{\partial v^0}{\partial y} + z\frac{\partial \theta_y^0}{\partial y} \\ \varepsilon_{zz} &= \frac{\partial w}{\partial z} = 0 \\ \gamma_{xy} &= \frac{\partial u}{\partial y} + \frac{\partial v}{\partial x} = \frac{\partial u^0}{\partial y} + \frac{\partial v^0}{\partial x} + z\frac{\partial \theta_x^0}{\partial y} + z\frac{\partial \theta_y^0}{\partial x} \\ \gamma_{yz} &= \frac{\partial v}{\partial z} + \frac{\partial w}{\partial y} = \frac{\partial w^0}{\partial y} + \theta_y^0 \\ \gamma_{xz} &= \frac{\partial u}{\partial z} + \frac{\partial w}{\partial x} = \frac{\partial w^0}{\partial x} + \theta_x^0 \end{aligned} \tag{13}$$

The transverse shear correction factor, typical of the first-order shear deformation theory, is assumed in the present work to be 5/6, as in Ref. [63], and shear-locking is minimized by selective/mixed integration schemes as employed by [62]. However, since electric potentials are assumed to be linear through thickness and only polarized in that direction, the electrical locking is not avoided. This is a similar approach to Refs. [64,65] and proved to effectively model the current study cases.

2.2. Double-Double laminates

The various lamination schemes can be implemented at the material level, the layer orientation level, or a combination of both. Lamination schemes based on stacking order and orientation are of particular interest when focusing the analysis on the purely elastic part of in-plane laminates. Due to the directional properties of the layers, the transformations associated with their stacking angles are essential for analyzing their mechanical behavior [66]. According to Ref. [53], at least four stiffness parameters are needed to define the stiffness of an orthotropic layer and consequently of the laminate. The Tsai Modulus, also known as trace, in the case of plane stress may be given as:

$$Trace\ 2D = tr(Q) = \tilde{Q}_{11} + \tilde{Q}_{22} + \tilde{Q}_{66} \tag{14}$$

The trace may define the behavior of composite laminates, since it can be considered as a representative of the stiffness of the respective material, defining the total potential stiffness [50]. As it is a linear combination of the three terms, if two are determined, the third will remain. This approach simplifies the determination of composite properties since two uniaxial tests, together with the trace, can define the properties, avoiding more difficult tests, such as shear tests [32,50]. This parameter also simplifies the design of structures, for instance, to achieve a 10% increase in stiffness for a laminate one may select a composite material with a trace value 10% higher [53]. This advantage is mainly valid for CFRPs as illustrated in Ref. [41] using the concept of master-ply and the stiffness components normalized by trace and thickness. The master-ply proposed by Tsai and Melo [32], is defined by an average of the stiffness matrices normalized by the trace and is considered to be a representative parameter of all CFRPs [39]. This consideration comes from the fact that the normalized stiffness coefficients show very little variation [32,41]. As shown by Ref. [39], it is possible to simplify the design of CFRP laminates by initially considering only master-ply as the base material and then using trace as the scaling factor for the structure's stiffness.

The normalization of a stiffness constant by the trace is obtained by the quotient between a given stiffness coefficient and the trace of the respective material. Thickness normalization is obtained by the quotient between a given stiffness coefficient and the thickness of a layer or laminate. Both normalizations are useful as they allow a direct comparison between materials since the coefficients now represent intensities independent of geometry and physical quantities [52]. According to Ref. [66], the thickness normalization of the matrices [A,B,D] defined in Eq. (11) is shown in Eq. (15) and defined by the superscript "*." The respective normalization by trace is shown in Eq. (16) and is defined by the superscript "**." Note that trace normalization can also be applied to the

stiffness coefficients Q_{ij} and the material properties (E_i, G_{ij}).

$$[A]^* = \frac{[A]}{h}; [B]^* = \frac{2}{h^2}[B]; [D]^* = \frac{12}{h^3}[D] \tag{15}$$

$$[A]^{**} = \frac{[A]^*}{tr(Q)}; [B]^{**} = \frac{[B]^*}{tr(Q)}; [D]^{**} = \frac{[D]^*}{tr(Q)} \tag{16}$$

According to Ref. [50], the integrations represented in Eq. (11) can be carried out in various ways, one of which is the multiple angle method. In this method, the coefficients of the matrices [*A*, *B*, *D*] are defined as functions of the lamination parameters [*V*, *Y*, *W*]. Thus, the normalized matrices $[A]^*$, $[B]^*$ and $[D]^*$ are defined according to Eqs. (17) and (18).

$$\left(\begin{Bmatrix} A_{11}^* \\ A_{22}^* \\ A_{12}^* \\ A_{66}^* \\ A_{16}^* \\ A_{26}^* \end{Bmatrix}, \begin{Bmatrix} B_{11}^* \\ B_{22}^* \\ B_{12}^* \\ B_{66}^* \\ B_{16}^* \\ B_{26}^* \end{Bmatrix}, \begin{Bmatrix} D_{11}^* \\ D_{22}^* \\ D_{12}^* \\ D_{66}^* \\ D_{16}^* \\ D_{26}^* \end{Bmatrix}\right) = \begin{bmatrix} U_1 & U_2 & U_3 & 0 & 0 \\ U_1 & -U_2 & U_3 & 0 & 0 \\ U_4 & 0 & -U_3 & 0 & 0 \\ U_5 & 0 & -U_3 & 0 & 0 \\ 0 & 0 & 0 & U_2/2 & U_3 \\ 0 & 0 & 0 & U_2/2 & -U_3 \end{bmatrix} \left(\begin{Bmatrix} 1 \\ V_1^* \\ V_2^* \\ V_3^* \\ V_4^* \end{Bmatrix}, \begin{Bmatrix} 1 \\ Y_1^* \\ Y_2^* \\ Y_3^* \\ Y_4^* \end{Bmatrix}, \begin{Bmatrix} 1 \\ W_1^* \\ W_2^* \\ W_3^* \\ W_4^* \end{Bmatrix}\right) \tag{17}$$

$$(\{V^*\}, \{Y^*\}, \{W^*\})_{[1,2,3,4]} = \left(\frac{1}{h}, \frac{2}{h^2}, \frac{12}{h^3}\right) \int_{-\frac{h}{2}}^{\frac{h}{2}} [\cos 2\theta, \cos 4\theta, \sin 2\theta, \sin 4\theta](1, z, z^2) dz \tag{18}$$

As first presented by Ref. [44] and more recently by Ref. [53], when a quasi-homogeneous laminate is achieved, $[A]^* = [D]^*$ and $[B]^* = 0$ are obtained. However, it should be noted that when computing the $[A]^* = [D]^*$ and $[B]^*$ matrices for each of these DD stacks, $[A]^*$ and $[D]^*$ and $[B]^*$ are not exactly zero. By increasing the number of repetitions, the components of $[D]^*$ tend to become equal to those of $[A]^*$, and those of $[B]^*$ become negligible. Regarding this matter, Ref. [41] introduced the concept of search propagation direction to model the stack recovery phase and ensure compliance with blending constraints, regardless of the orientation values and positions of dropped plies within the laminates. The solutions obtained satisfy the membrane/bending uncoupling ($[B]^* = 0$) and homogeneity ($[A]^* = [D]^*$) conditions, regardless of the value of the orientation angles, along with their respective residuals associated with the solution.

The lamination parameters V^* and W^* for the matrices $[A]^*$ and $[D]^*$ are so given as follows [34,53]:

$$\begin{aligned} V_1^* &= \frac{(A_{11}^* - A_{22}^*)}{2U_2}; V_2^* = \frac{A_{11}^* + A_{22}^* - 2U_1}{2U_3}; \\ V_3^* &= \frac{(A_{61}^* + A_{62}^*)}{U_2}; V_4^* = \frac{(A_{61}^* - A_{62}^*)}{2U_3} \end{aligned} \tag{19}$$

$$\begin{aligned} W_1^* &= \frac{(D_{11}^* - D_{22}^*)}{2U_2}; W_2^* = \frac{D_{11}^* + D_{22}^* - 2U_1}{2U_3}; \\ W_3^* &= \frac{(D_{61}^* + D_{62}^*)}{U_2}; W_4^* = \frac{(D_{61}^* - D_{62}^*)}{2U_3} \end{aligned} \tag{20}$$

Considering Double-Double laminates, their possible combinations are shown in Eq. (21). Note that this approach is field-based—varies continuously from 0 to 90°—and not discrete, as a collection of laminates [20,29].

$$\begin{aligned} &Staggered\ 1 = [+\Phi|-\Psi|-\Phi|+\Psi] \\ &Staggered\ 2 = [+\Phi|+\Psi|-\Phi|-\Psi] \\ &Staggered\ 3 = [+\Phi|-\Psi|+\Psi|-\Phi] \\ &Staggered\ 4 = [+\Phi|+\Psi|-\Psi|-\Phi] \\ &Paired\ 1 = [+\Phi|-\Phi|+\Psi|-\Psi] \\ &Paired\ 2 = [+\Phi|-\Phi|-\Psi|+\Psi] \end{aligned} \tag{21}$$

According to Ref. [53], the lamination parameters V^* for DD laminates are given as follows:

$$\begin{aligned} V_1^* &= \big(\cos 2\Phi + \cos(-2\Phi) + \cos 2\Psi + \cos(-2\Psi)\big)/4 \\ &= (\cos 2\Phi + \cos 2\Psi)/2 \\ V_2^* &= \big(\cos 4\Phi + \cos(-4\Phi) + \cos 4\Psi + \cos(-4\Psi)\big)/4 \\ &= (\cos 4\Phi + \cos 4\Psi)/2 \\ V_3^* &= \sin 2\Phi + \sin(-2\Phi) + \sin 2\Psi + \sin(-2\Psi) = 0 \\ V_4^* &= \sin 4\Phi + \sin(-4\Phi) + \sin 4\Psi + \sin(-4\Psi) = 0 \end{aligned} \tag{22}$$

Considering the relationships expressed in Eq. (22) and after the respective mathematical manipulations, the calculation of the fiber orientations for the DD using the V_i lamination parameters is carried out according to Eq. (23).

$$\begin{aligned} \cos 2\Psi &= V_1^* + \sqrt{(-V_1^*)^2 + (V_2^*/2) + (1/2)} \\ \cos 2\Phi &= 2V_1^* - \cos 2\Psi \end{aligned} \tag{23}$$

The conversion of conventional or unconventional laminates to DD can be done directly for the $[A]^*$ or $[D]^*$ matrix using the respective V_i, W_i parameters. According to Ref. [53], the calculation of the angles for the DD can be carried out from three different stages as summarized in Figure 1.

More on the mathematical interpretation of the DD, in its extensive format, can be found in Ref. [53].

2.3. Finite element formulation

The finite element used in this work—referred to as Q4FSDT—is a four-node, bilinear displacement Lagrange element based on the first-order shear deformation theory considering an equivalent single layer approach for the mechanical displacement with a layerwise-type approximation for the electric potential. Therefore, this element has twenty mechanical degrees of freedom per element and one electrical degree of freedom per element/active layer.

The behavior of a hybrid piezoelectric laminated composite can be obtained using a variational approach *via* the principle of virtual work and the governing equation of motion can be presented as follows [61,62]:

$$\iiint_V \left\{\delta\varepsilon^T \overline{Q}\varepsilon - \delta\varepsilon^T \overline{e}E - \delta E^T \overline{e}^T \varepsilon - \delta E^T \overline{\epsilon} E + \rho \delta u^T \ddot{u}\right\} dV\text{-}\delta W_u + \delta W_\phi = 0 \tag{24}$$

where δW_u and δW_ϕ are, respectively, the virtual work done by the mechanical external forces and the applied surface charge. The governing equations of equilibrium of the discretized domain are obtained after the proper mathematical manipulation of the constitutive equations and the principle of virtual work. Considering the electromechanical static case, Eqs. (25) and (26) apply as described by [58]:

$$\begin{aligned}[K_{uu}]\{u\} + [K_{u\phi}]\{\phi\} &= \{F_u\} \\ [K_{\phi u}]\{u\} + [K_{\phi\phi}]\{\phi\} &= \{F_\phi\}\end{aligned} \tag{25}$$

$$\{F_a\} = [K_{u\phi}]\{\phi\} \tag{26}$$

where $[K_{uu}], [K_{u\phi}], [K_{\phi u}]$, and $[K_{\phi\phi}]$ are the pure elastic stiffness, elastic and electric coupling effects, and pure electric contributions matrices; $\{u\}, \{\phi\}, \{F_u\}$, and $\{F_\phi\}$ are the generalized electromechanical response of the structure and load vectors; $\{F_a\}$ is the equivalent mechanical force vector that adds up to $\{F_u\}$ due to the voltage ϕ applied to the actuators.

Depending on the type of Mechanical Boundary Conditions (MBCs) and Electric Boundary Conditions (EBCs), the form of the equation will adapt, e.g. for closed circuit sensory function only the elastic part of the equations is considered. According to Refs. [64,65], for the dynamic case (free harmonic vibrations) the following Eqs. (27) and (28) apply:

$$\begin{aligned}\left([K_{uu}] + \{\omega_n\}^2[M_{uu}]\right)\{u\} + [K_{u\phi}]\{\phi\} &= 0 \\ [K_{\phi u}]\{u\} + [K_{\phi\phi}]\{\phi\} &= 0\end{aligned} \tag{27}$$

The eigenvalue/vector problem is then solved by considering the EBCs, either open or closed circuits as given as follows:

$$\begin{aligned}&\left([K^*] + \{\omega_n\}^2[M_{uu}]\right)\{u\} = 0 \\ &[K^*] = \begin{cases}[K_{uu}] & \text{if closed} \\ [K_{uu}] - [K_{u\phi}][K_{\phi\phi}]^{-1}[K_{\phi u}] & \text{if open}\end{cases}\end{aligned} \tag{28}$$

where, $[M_{uu}]$ is the mass matrix and $\{\omega_n\}$ corresponds to each natural frequency, associated with the mode n.

Within this work, we considered several MBCs presented throughout the sections and EBCs as presented in Figure 2. Under Simply Supported (S) conditions, vertical displacements are constrained, while rotation remains unrestricted. Conversely, in Clamped (C) configurations, all displacements and rotations are effectively restricted. Lastly, in Free-edge (F) scenarios, no constraints are imposed on displacements or rotations. The sequence of four characters, for example, CSCF, means that for a rectangular plate, the border $x = 0$ is Clamped, the border $x = a$ is Simply Supported, the border $y = 0$ is Clamped and the border $y = b$ is Free. A comprehensive definition of the MBCs imposed is described [62].

Regarding EBCs, under closed-circuit (or sensory) conditions, the structural behavior is solely evaluated based on its mechanical aspects, and electric potentials at the external surfaces of the piezoelectric patches are enforced to be zero. Conversely, under open-circuit conditions, both mechanical and electrical contributions are considered. In the open circuit, electric potentials are left unrestricted at the external surfaces, allowing for a less constrained electric potential field. This less constrained field leads to induced stiffness and consequently increases the natural frequencies of the structure [58].

3. Numerical results and discussion

In this section, a set of performance assessment and verification cases, and case studies are conducted, comprising beam and plate structures to characterize the performance of the proposed model and study the influence of the several stacking sequences in different scenarios.

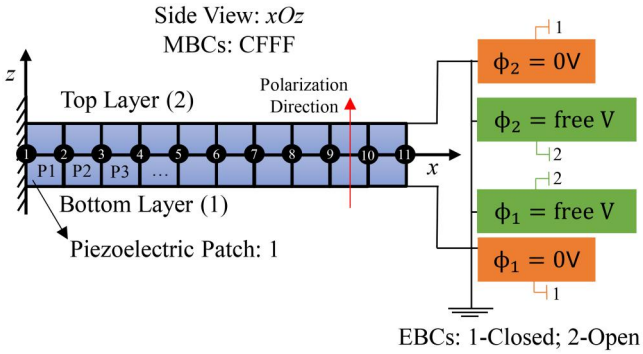

Figure 2. Representation of EBCs in open and closed-circuit: Cantilever piezoelectric bimorph.

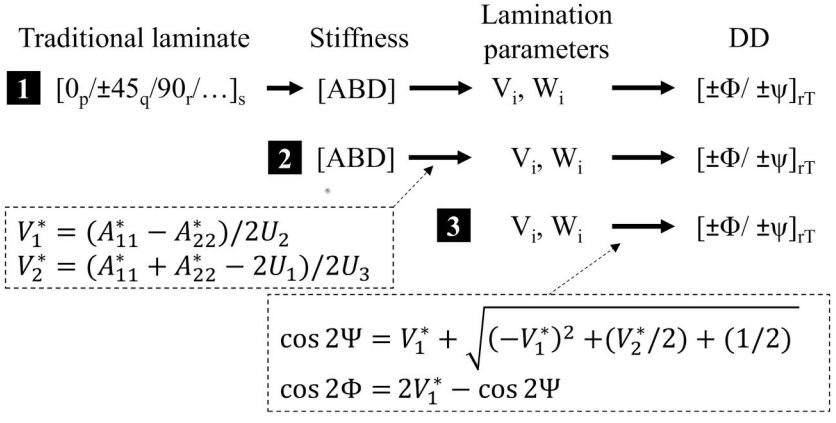

Figure 1. Presentation of the three options for calculating the angles for the DD. Adapted from Ref. [53].

3.1. Performance assessment and verification studies

To evaluate the performance of the implemented model, it is necessary to compare it with other approaches and theories, as extensively covered in Refs. [67,68]. In this section, we consider again a hybrid piezoelectric sandwich plate that consists of a symmetric three-layer cross-ply (0/90/0) graphite/epoxy laminate core and two 0.1 h-thick piezoceramic layers, as presented in Refs. [2,68]. The EBCs are those of a Closed Circuit and the MBCs are those of a simply supported plate. Both thin and thick plates (thickness ratio, L/h) have been analyzed, and as presented in Ref. [68], reduced selective integration (SI) has been carried out alongside the conventional normal integration (NI) to address the effects of the shear locking phenomenon. The properties of the materials under consideration are detailed in Table 1. However, it should be noted that in this case, the density (ρ) has a unit value for both materials.

Here, the current formulation is compared to ESL and LW, employing expansion orders of 1 and 4, respectively, utilizing Q9 elements based on Carrera's Unified Formulation (CUF). The comparisons are listed in Table 2, and Table 3 extends the study, presenting results for the Open-Circuit mode by showing the stiffening effect of the structure due to the electromechanical effect.

On observing the results obtained and particularly from Table 2, the comparisons with different element formulations, including ED1, ED4, and layer-wise descriptions highlight the significance of the order of expansion in the formulation, on result accuracy. Higher-order elements and layer-wise descriptions outperform lower-order elements although a finer mesh resolution can lead to acceptable

Table 1. Material properties for the performance assessment case.

Piezoelectric layers (PZT-4)	$E_1 = E_2 = 81.3$ GPa, $E_3 = 64.5$ GPa, $\nu_{23} = \nu_{13} = 0.43$, $\nu_{12} = 0.33$, $G_{23} = G_{13} = 25.6$ GPa, $G_{12} = 30.6$ GPa, $d_{31} = d_{32} = -122$E-12 m/V, $d_{33} = -285$E-12 m/V, $\epsilon_{33} = 115.05$E-10 F/m, $\rho_{PZT\text{-}4} = 7600$ kg/m^3
Graphite-epoxy layers	$E_1 = 132.38$ GPa, $E_2 = E_3 = 10.76$ GPa, $G_{23} = 3.61$ GPa, $G_{13} = G_{12} = 5.65$ GPa, $\nu_{23} = 0.49$, $\nu_{12} = \nu_{13} = 0.24$, $\rho_{Gr\text{-}Ep} = 1578$ kg/m^3

Table 2. Comparison of the first three thickness circular frequencies (ω/100 rad/s) for the hybrid sandwich plate.

CC	L/h	4			50		
Ref	Mode	1	2	3	1	2	3
3D Exact [73]		57,074.5	191,301	250,769	618.118	15,681.6	21,492.8
2D CF [74]		58,216.1	196,018	268,650	618.435	15,684	21,499.4
LD4	SI	57,096.9	191,361	250,803	618.450	15,686.9	21,560.4
Q9 (4 × 4)	NI	57,116.9	191,364	250,815	624.635	16,686.9	21,497.3
[68]	CF	57,074	191,301	250,768	618.104	15,681.6	21,492.6
LD1	SI	57,275.5	194,907	255,689	619.473	15,688.8	21,499.2
Q9 (4 × 4)	NI	57,296.9	194,908	255,698	625.584	15,688.8	21,499.2
[68]	CF	57,252.5	194,840	255,646	619.022	15,683.4	21,499.4
ED4	SI	58,740.3	194,660	254,787	618.913	15,698.9	21,502.5
Q9 (4 × 4)	NI	58,765.7	194,662	254,798	625.190	15,698.9	21,502.5
[68]	CF	58,713.8	194,592	254,740	618.464	15,693.5	21,497.8
ED1	SI	74,232.1	195,842	266,411	690.338	15,700.3	21,512.7
Q9 (4 × 4)	NI	74,249.8	195,930	262,271	688.575	15,700.2	21,510
[68]	CF	74,105.9	196,021	266,337	689.867	15,695.0	21,498.5
Q4FSDT	(4 × 4)	67,074.102	197,679.222	261,293.977	628.168	16,093.301	21,425.071
SI	(8 × 8)	65,359.729	197,131.200	258,722.170	596.211	15,769.736	21,073.804
	(10 × 10)	65,148.492	195,891.525	252,106.530	592.433	15,671.322	21,031.517
	(16 × 16)	64,918.591	195,288.579	246,569.634	588.381	15,623.086	20,985.691
	(20 × 20)	64,865.388	195,149.733	245,336.260	587.452	15,611.979	20,975.114
Q4FSDT	(4 × 4)	69,004.887	201,166.262	261,293.977	1912.519	15,634.903	21,425.071
NI	(8 × 8)	65,815.136	199,608.774	257,215.555	1054.212	15,715.993	21,073.804
	(10 × 10)	65,438.013	195,891.525	252,106.530	911.229	15,671.322	21,031.517
	(16 × 16)	65,030.878	195,288.578	246,569.634	729.103	15,623.086	20,985.691
	(20 × 20)	64,937.135	195,149.733	245,336.260	680.796	15,611.979	20,975.114

Closed circuit mode.
Note: CF refers to closed form solution.

Table 3. First three thickness circular frequencies (ω/100 rad/s) for the hybrid sandwich plate.

	L/h	4			50		
OC	Mode	1	2	3	1	2	3
Q4FSDT	(4 × 4)	67,862.932	197,707.206	261,956.430	643.176	16,133.147	21,631.401
SI	(8 × 8)	66,192.148	198,263.571	258,722.398	609.922	15,945.665	21,286.093
	(10 × 10)	65,985.619	196,374.085	252,106.530	606.106	15,709.927	21,244.446
	(16 × 16)	65,760.694	195,769.362	246,569.634	602.013	15,695.036	21,303.719
	(20 × 20)	65,708.621	195,630.107	246,175.682	601.075	15,650.409	21,188.871
Q4FSDT	(4 × 4)	69,770.781	201,664.332	261,956.430	1916.691	15,642.518	21,631.401
NI	(8 × 8)	66,640.904	200,717.119	257,215.555	1061.828	15,754.729	21,286.093
	(10 × 10)	66,270.815	196,374.085	252,106.530	920.032	15,709.927	21,229.285
	(16 × 16)	65,871.263	195,769.362	246,569.634	740.078	15,662.078	21,199.295
	(20 × 20)	65,779.264	195,630.108	246,175.682	692.538	15,650.409	21,188.871

Open circuit mode.

solutions. Specifically, the difference between the number of nodes in Q9 (ED1) and Q4FSDT can be surpassed by employing a much finer mesh. However, it is important to mention that the order of expansion has different implications on the results, being more noticeable in the ESL elements than in LW elements. The effect and minimization of shear locking through the type of integration employed are also observed. In general, all the LW elements performed better than ESL ones even for higher order ESL elements. Thus, it is necessary to consider that although the results are acceptable for certain cases, there are many limitations in using elements with few nodes, linear shape functions, and linear interpolation.

The primary challenge in multilayered piezoelectric constructions arises from the potential variation in mechanical and electrical properties along the thickness direction. Anisotropic multilayered composites often demonstrate higher transverse shear and transverse normal flexibilities compared to traditional isotropic single-layered ones, complicating the application of plate theories like Kirchhoff's hypothesis or Reissner–Mindlin theory (FSDT and CLT) [69]. These theories may not adequately capture the static and dynamic responses of piezoelectric plates due to the increased transverse deformability, necessitating consideration of transverse shear and normal stresses often neglected in classical analyses. Moreover, the discontinuity in mechanical properties across layers results in displacement fields that undergo abrupt changes in slope at layer interfaces, known as the Zig-Zag (ZZ) effect [68–70]. However, for equilibrium considerations, Interlaminar Continuity (IC) is required for transverse stresses and several discussions by Refs. [12,68,71] have addressed theories dealing with ZZ and IC. Regarding electrical variables, it is essential to note that an accurate representation of electrical stiffnesses requires a linear distribution of the electric field through the thickness of the piezoelectric layers [69]. Consequently, assuming a parabolic distribution for the electric potential within the layers becomes necessary [2,68].

The comparisons made in this section are with CUF, which emerged as a generalized approach to generate any expansions for structural theories [13] and being a hierarchical formulation, considers the order of the models as a free parameter of the analysis [69]. Therefore, permits to develop a large number of structural theories with a variable number of displacement unknowns using a succinct notation and by referring to a few fundamental nuclei [72].

Future developments in the present work will focus on the implementation of this approach.

Following the previous assessment studies, one proceeded to the static and free vibration responses characterization, where the results obtained are studied and compared with other results available in the literature with both analytical and numerical solutions. The first verification case carried out focuses on the purely elastic part of the material and considers a typical simply supported, square composite laminated plate subject to Uniformly Distributed Loads (UDL) as presented by Reddy [62]. The plate edge dimension is unitary, and the material properties used are given in Table 4 both for the linear static and free vibration analysis. The shear correction factor was fixed to $K_s = 5/6$.

For the free vibration verification study, several 10-angle-ply laminates with different MBCs are verified under the free vibration dynamic state as studied by Khdeir [75]. In both studies, the discretization used is a (20 × 20) mesh and the dimensionless results are given in Tables 5 and 6.

Then to verify the piezoelectric effect, a typical cantilevered piezoelectric bimorph beam with two PVDF layers bonded together is considered. They are polarized in

Table 4. Material properties for first verification case.

Linear static analysis	$E_1 = 25\ E_2$	$G_{12} = G_{13} = 0.5\ E_2$	$G_{23} = 0.2\ E_2$	$\nu_{12} = 0.25$
Free vibration analysis	$E_1 = 40\ E_2$	$G_{12} = G_{13} = 0.6\ E_2$	$G_{23} = 0.5\ E_2$	$\nu_{12} = 0.25$

Table 5. Comparison of dimensionless deflections ($\bar{w} = w(E_2h^3/b^4q_0)$) of cross-ply and angle-ply laminates.

	Cross-ply				Angle-Ply			
	Symmetric		Antisymmetric		Antisymmetric		Antisymmetric	
	[0/90/90/0]		$[0/90]_4$		[-45/45]		$[-45/45]_4$	
L/h	[62]	Q4FSDT (20 × 20)	[62]	Q4FSDT (20 × 20)	[62]	Q4FSDT (20 × 20)	[62]	Q4FSDT (20 × 20)
10	1.0250	1.0255	0.9660	0.9660	1.2792	1.2797	0.6366	0.6375
20	0.7694	0.7676	0.7776	0.7768	1.0907	1.0904	0.4483	0.4483
100	0.6833	0.6825	0.7175	0.7165	1.0305	1.0300	0.3883	0.3881

Table 6. Comparison of dimensionless fundamental frequencies ($\bar{\omega} = \omega \times L^2 \times (\sqrt{\rho/E_2})/h$) of angle-ply laminates.

MBCs	SSSS		SSSC		SSCC		SSFF	
θ	[75]	Q4FSDT (20 × 20)	[75]	Q4FSDT (20 × 20)	[75]	Q4FSDT (20 × 20)	[75]	Q4FSDT (20 × 20)
30	18.51	18.54	19.11	19.16	19.81	19.85	10.11	10.14
45	19.38	19.41	20.27	20.31	21.25	21.29	6.57	6.59
60	18.51	18.53	19.82	19.86	21.21	21.24	3.82	3.84

Table 7. Material properties for the second verification case.

E1 = E2 = E3	G23 = G13 = G12	$\nu23 = \nu13 = \nu12$	e31 = e32	e33	ϵ_{33}
2 GPa	1 GPa	0	0.046 C/m^2	0 C/m^2	1.062E-10 F/m

Table 8. Cantilever piezoelectric bimorph beam.

Ref	Mode	Location, x (m) Element	20E-3 1	40E-3 2	60E-3 3	80E-3 4	100E-3 5
[61]	Actuator	Deflection	0.138E-7	0.552E-7	1.240E-7	2.210E-7	3.450E-7
Q4FSDT			0.138E-7	0.552E-7	1.240E-7	2.210E-7	3.450E-7
[61]	Sensor	Voltage	290	226	161	97	32
Q4FSDT			295	229	164	98	32

Deflections in [m]; sensed voltage in [V].

Table 9. Material properties for the third verification case.

Piezoelectric layers	E1 = E2 = E3 = 2 GPa; $\nu23 = \nu13 = \nu12 = 0.29$, e31 = e32 = 0.0046 C/m^2, e33 = 0 C/m^2, ϵ_{33} = 1.062E-10 F/m
Inner layers	E2 = 6.9 GPa, E1/E2 = 25, G13 = G12 = 0.5E2, G23 = 0.2E2, $\nu23 = \nu13 = \nu12 = 0.25$

Table 10. Simply supported hybrid composite plate ([p/0°/90°/0°/p).

					L/h = 4		L/h = 50	
Static, $\bar{w}\left(\frac{L}{2}, \frac{L}{2}, 0\right)$	L/h = 10	L/h = 20	L/h = 100	Dynamic, 1st mode, $\bar{\omega}$	CC	OC	CC	OC
[76]	0.6690	0.4920	0.4330	[77]	145.323	151.222	236.833	259.173
Q4FSDT	0.6640	0.4897	0.4323	Q4FSDT	166.437	168.557	237.225	242.680

Non-dimensional maximum deflections ($100wE_2h^3/q_0L^4$) and non-dimensional fundamental frequencies ($\omega L^2/(h\times\sqrt{\rho}\times10^3)$) Hz(kg/m)$^{1/2}$.

opposite directions as in Ref. [61] and have a length ($L = 0.1$ m), width ($b = 0.005$ m), and height ($h_{\max} = 0.001$ m). The material properties used are presented in Table 7.

In the actuator case, the upper and lower surfaces of the bimorph beam are subjected to a unit electrical potential (±0.5 V), and for the sensor mode, a tip deflection of 10 mm is imposed. In both studies, the discretization used is a (1 × 5) mesh and the results obtained are given in Table 8.

Next, a five-ply, simply supported, square sandwich laminated plate with surface bonded piezoelectric layers ([p/0°/90°/0°/p], $h_{\text{core}} = 3$ mm, $h_{\text{piezo}} = 40\,\mu$m) is considered. In the static scenario of Ref. [76], the laminate is subjected to a doubly sinusoidal loading (SDL), and the piezoelectric layers are considered isotropic with a null voltage. The material properties used for the outer piezoelectric layers and for the inner ones are presented in Table 9.

In the dynamic scenario, the same lamination sequence is considered with three plies of Graphite/Epoxy ($h_{\text{core}} = 0.8h_{\text{total}}$) and two PZT-4 piezoelectric layers ($h_{\text{piezo}} = 0.1h_{\text{total}}$) with unit edge length [76]. The material properties used are the ones presented in Table 1.

Two different EBCs conditions were then analyzed: Closed-Circuit (CC), where the electric potential is null, and Open Circuit (OC), where the electric potential remains free. For the static case, the discretization considered is a (20 × 20) mesh and for the dynamic case is (8 × 8) similar to Ref. [77]. To compare with the reference results, one considers unit density. The results obtained in these two studies are given in Table 10.

Finally, regarding the DD approach, the replacement of a QUAD by a DD and the homogenization is verified. The QUAD considered was a general laminate in IM6/Epoxy as considered by Ref. [53] with a total of 72 layers, 9 mm of thickness, and the stacking sequence: $[0_3/45/90_2/-45_3/0/-45/45_2/90/45/-45/0/45]_{2S}$. Note that in this case the shear correction factor is considered unitary, $K_s = 1$. The DD replacement of the QUAD obtained to match the in-plane stiffness is $(\pm62, \pm20)_{18}$ and to match the flexural stiffness is $(\pm61, \pm14)_{18}$. The results are given in Tables 11 and 12, respectively.

Table 11. Equivalent DD laminate to conventional QUAD in [A]*.

		Φ		Ψ	rT
DD laminate [A]* equivalent		62°		20°	18
Reference	(GPa)	[A]* QUAD	[A]* DD	[D]* QUAD	[D]* DD
[53]	11	94.2	94.2	104.6	94.2
Q4FSDT		94.1734	93.6643	104.5823	93.6643
[53]	22	72.7	72.7	70.3	72.7
Q4FSDT		72.7413	73.7145	70.3338	73.7145
[53]	21	27.9	27.9	23.9	27.9
Q4FSDT		27.8555	27.6235	23.8548	27.6235
[53]	66	32.7	32.7	28.7	32.7
Q4FSDT		32.6512	32.4191	28.6505	32.4191
[53]	61	0	0	−1.8	0
Q4FSDT		0	0	−1.8480	0.0836
[53]	62	0	0	−1.8	0
Q4FSDT		0	0	−1.8480	0.0807

For all the verification studies, the results observed prove to have a good agreement between the present finite element model and the reference results. Regarding the laminate conversion, the results obtained for the [A]*, [B]*, and [D]* matrices of the QUAD laminate show that they are not homogeneous since [A]* ≠ [D]* and because of the presence of shear coupling for the bending stiffness. It is important to note that while the DD laminate may be a replacement for the initial QUAD, it is not precisely identical.

3.2. Case studies

In this section, two case studies regarding hybrid laminates are presented: "Lamination schemes: QUAD *vs.* DD" and "Tapering of Laminated structures"—examining both static and dynamic aspects of behavior. One notes that the result tables have conditional formatting styles (coloring) to help visualize the results. Thus, in the green-red color gradient, green corresponds to lower values and red to higher values, giving an idea of the evolution of the quantity in question.

Table 12. Equivalent DD laminate to conventional QUAD in $[D]^*$.

		Φ		Ψ	rT
DD laminate $[D]^*$ equivalent		61°		14°	18
Reference	(GPa)	$[A]^*$ QUAD	$[A]^*$ DD	$[D]^*$ QUAD	$[D]^*$ DD
[53]	11	94.2	104.6	104.6	104.6
Q4FSDT		94.1734	104.2249	104.5823	104.2249
[53]	22	72.7	70.3	70.3	70.3
Q4FSDT		72.7413	70.1771	70.3338	70.1771
[53]	21	27.9	23.9	23.9	23.9
Q4FSDT		27.8555	24.1119	23.8548	24.1119
[53]	66	32.7	28.7	28.7	28.7
Q4FSDT		32.6512	28.9075	28.6505	28.9075
[53]	61	0	0	−1.8	0
Q4FSDT		0	0	−1.8480	0.0718
[53]	62	0	0	−1.8	0
Q4FSDT		0	0	−1.8480	0.0753
		Φ	Ψ	Φ	Ψ
$[B]^*$, $rT = 18$		61°	14°	62°	20°
Reference	(GPa)	$[B]^*$ QUAD	$[B]^*$ DD	$[B]^*$ QUAD	$[B]^*$ DD
Q4FSDT	11	0	1.0975	0	0.9707
	22	0	−0.7951	0	−0.8045
	21	0	−0.1512	0	−0.0831
	66	0	−0.1512	0	−0.0831
	61	0	0.2702	0	0.4549
	62	0	−0.7773	0	−0.7043

The materials considered in these studies are PZT-4 [77] and IM6/Epoxy, and the corresponding properties are presented in Table 13.

3.2.1. Lamination schemes: QUAD vs. DD

The static and dynamic analysis of hybrid laminated plates featuring diverse lamination schemes under different CFs are addressed in the present case study. The lamination schemes considered are the same as the DD verification study, where a conventional QUAD laminate was converted to DD. Thus, the QUAD lamination scheme in IM6/Epoxy is $[0_3/45/90_2/-45_3/0/-45/45_2/90/45/-45/0/45]_{2S}$—with a total thickness of 9 mm. PZT-4 piezoelectric layers with a total thickness of 0.5 (mm) per layer were considered at the outer

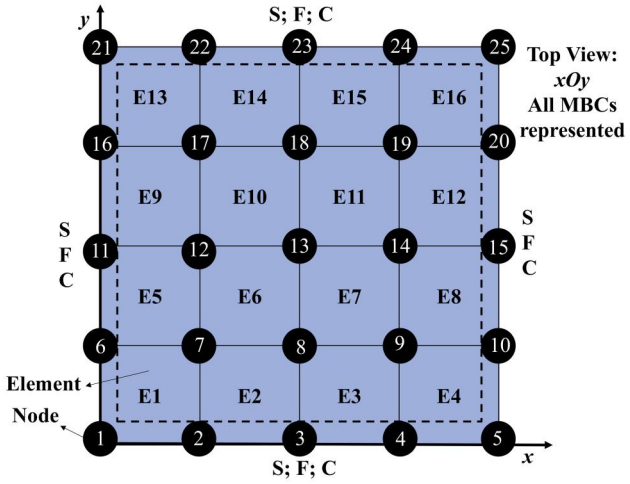

Figure 4. Top view of a typical plate (4 × 4 finite element discretization) representing all the MBCs: simply supported (S), clamped (C), and free-edge (F).

Table 13. Material coefficients and properties for the case studies.

PZT-4 layers	$\rho_{PZT\text{-}4} = 7600\ kg/m^3$, $Q_{11} = 1.385E11$ Pa, $Q_{12} = 7.7371E10$ Pa, $Q_{13} = 7.3643E10$ Pa, $Q_{22} = 1.385E11$ Pa, $Q_{23} = 7.3643E10$ Pa, $Q_{33} = 1.1475E11$ Pa, $Q_{44} = 2.56E10$ Pa, $Q_{55} = 2.56E10$ Pa, $Q_{66} = 3.06E10$ Pa, $\epsilon_{11} = 1.306E\text{-}8$ F/m, $\epsilon_{22} = 1.306E\text{-}8$ F/m, $\epsilon_{33} = 1.151E\text{-}8$ F/m, $e_{31} = -5.2\ C/m^2$, $e_{32} = -5.2\ C/m^2$, $e_{33} = 15.08\ C/m^2$
IM6/Epoxy layers	$\rho_{IM6/Epoxy} = 1536\ kg/m^3$, $Q_{11} = 2.0742E11$ Pa, $Q_{12} = 6.9096E9$ Pa, $Q_{13} = 6.9096E9$ Pa, $Q_{22} = 1.4606E10$ Pa, $Q_{23} = 6.9867E9$ Pa, $Q_{33} = 1.4606E10$ Pa, $Q_{44} = 3.8095E9$ Pa, $Q_{55} = 8.4E9$ Pa, $Q_{66} = 8.4E9$ Pa

Note that for both studies presented, the shear correction factor considered is 5/6.

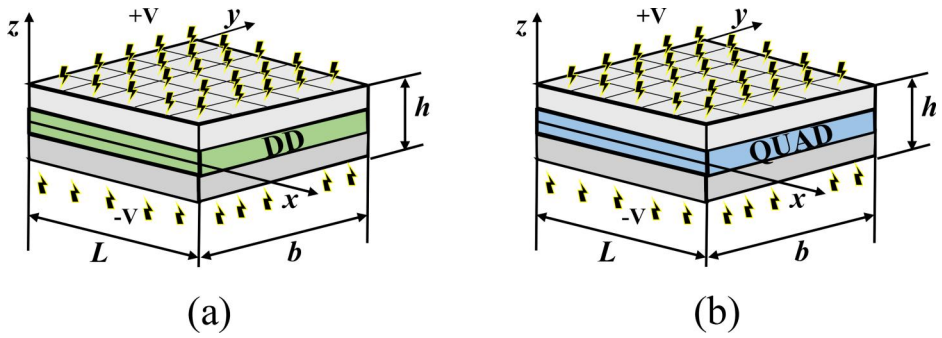

Figure 3. Schematic representation of the lamination schemes and the reference system considered: (a) Double-Double; (b) QUAD.

Table 14. Static response of hybrid QUAD and DD laminated plates with different boundary conditions: transverse displacement for actuator mode—sample results.

			Maximum displacement, w (μm)								
Lam/MBCs	[p/QUAD/p]	Equivalent	Stagg1	Stagg2	Stagg3	Stagg4	Paired1	Paired2	Average	Standard deviation	CV%
SSSS	3.257	[*D*]*	3.248	3.250	3.250	3.251	3.248	3.248	3.250	0.003	0.10
		[*A*]*	3.144	3.146	3.145	3.147	3.144	3.143	3.161	0.042	1.34
SSCC	0.805	[*D*]*	0.805	0.806	0.805	0.805	0.806	0.806	0.805	0.000	0.03
		[*A*]*	0.771	0.772	0.771	0.771	0.771	0.771	0.776	0.013	1.66
SSCS	2.014	[*D*]*	2.010	2.012	2.010	2.011	2.011	2.010	2.011	0.001	0.06
		[*A*]*	1.931	1.932	1.931	1.932	1.931	1.931	1.943	0.031	1.60
SSFF	4.710	[*D*]*	4.713	4.717	4.719	4.722	4.715	4.714	4.716	0.004	0.08
		[*A*]*	4.982	4.986	4.988	4.991	4.983	4.982	4.946	0.104	2.10
SSFC	2.523	[*D*]*	2.522	2.524	2.523	2.525	2.522	2.522	2.523	0.001	0.04
		[*A*]*	2.533	2.536	2.535	2.537	2.534	2.534	2.533	0.005	0.18
CCFF	−1.717	[*D*]*	−1.716	−1.716	−1.716	−1.716	−1.716	−1.716	−1.716	0.001	0.03
		[*A*]*	−1.700	−1.700	−1.700	−1.700	−1.700	−1.700	−1.702	0.006	0.38

CV: percentage coefficient of variation, %.

The tables utilize conditional formatting styles to vividly illustrate the results. Within the green-red color spectrum, lower values are represented by shades of green while higher values are depicted in red. This colour gradient is an attempt to offer a clear depiction of the progression of the relevant physical quantity.

Table 15. Dynamic response of hybrid QUAD and DD plates in free vibration (closed/open sensor mode)—sample results.

		Fundamental frequency, ω (Hz)																			
Lam		[p/QUAD/p]		Stagg1		Stagg2		Stagg3		Stagg4		Paired1		Paired2		OC			CC		
MBCs		OC	CC	OC	CC	OC	CC	OC	CC	OC	CC	OC	CC	OC	CC	Average	Std. Dev	CV%	Average	Std. Dev	CV%
SSSS	[*D*]*	638.788	632.547	639.458	633.226	639.292	633.056	639.373	633.139	639.248	633.011	639.456	633.223	639.497	633.266	639.302	0.244	0.04	633.067	0.248	0.04
	[*A*]*			648.457	642.321	648.246	642.106	648.375	642.237	648.216	642.075	648.450	642.313	648.503	642.367	647.005	3.625	0.56	640.852	3.664	0.57
SSCC	[*D*]*	894.281	885.384	894.208	885.326	893.973	885.087	894.331	885.450	894.155	885.270	894.017	885.131	894.076	885.191	894.149	0.134	0.01	885.263	0.134	0.02
	[*A*]*			908.222	899.511	907.912	899.194	908.340	899.629	908.107	899.392	908.009	899.294	908.087	899.373	906.137	5.23	0.58	897.397	5.299	0.59
SSCS	[*D*]*	748.049	740.635	748.460	741.057	748.259	740.852	748.474	741.070	748.323	740.916	748.363	740.958	748.413	741.009	748.334	0.147	0.02	740.928	0.151	0.02
	[*A*]*			760.045	752.775	759.783	752.507	760.057	752.786	759.860	752.585	759.935	752.663	760.001	752.729	758.247	4.498	0.59	750.954	4.552	0.61
SSFF	[*D*]*	338.330	336.355	337.781	335.807	337.746	335.771	337.575	335.599	337.549	335.572	337.766	335.791	337.774	335.800	337.789	0.258	0.08	335.813	0.258	0.08
	[*A*]*			322.855	320.830	322.822	320.794	322.686	320.659	322.661	320.632	322.857	320.830	322.865	320.839	325.011	5.874	1.81	322.991	5.894	1.82
SSFC	[*D*]*	423.630	421.518	423.592	421.482	423.508	421.395	423.439	421.327	423.376	421.262	423.553	421.441	423.574	421.463	423.525	0.09	0.02	421.413	0.091	0.02
	[*A*]*			417.720	415.602	417.618	415.497	417.587	415.468	417.511	415.389	417.691	415.571	417.716	415.598	418.496	2.265	0.54	416.377	2.268	0.54
CCFF	[*D*]*	762.054	756.759	761.328	756.021	761.205	755.895	760.959	755.649	760.867	755.554	761.062	755.750	761.093	755.781	761.224	0.396	0.05	755.915	0.402	0.05
	[*A*]*			731.540	726.020	731.407	725.883	731.235	725.712	731.135	725.609	731.325	725.799	731.358	725.833	735.722	11.612	1.58	730.231	11.699	1.60

CV%: percentage coefficient of variation, %.

The tables utilize conditional formatting styles to vividly illustrate the results. Within the green-red color spectrum, lower values are represented by shades of green while higher values are depicted in red. This colour gradient is an attempt to offer a clear depiction of the progression of the relevant physical quantity.

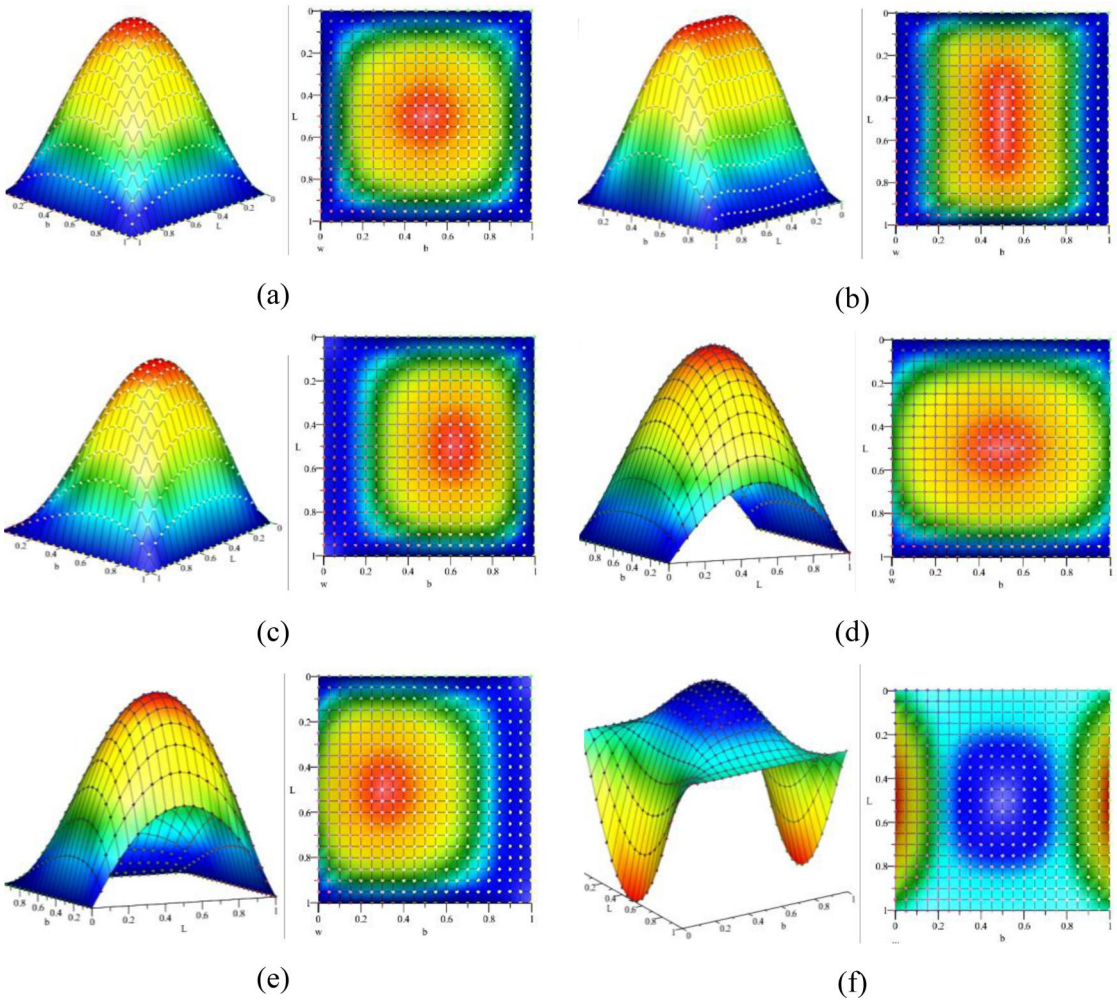

Figure 5. Actuating mode shapes under different MBCs: (a) SSSS, (b) SSCC, (c) SSCS, (d) SSFF, (e) SSFC, (f) CCFF.
Note: Side dimensions are normalized as (*x*/*L*; *y*/*L*).

layers of the structure with the total thickness of the structure being 10 mm and $L/h = 30$. The DDs considered are the equivalents obtained for $[D]^*$ and $[A]^*$, i.e. $(\Phi, \psi) = (\pm 61, \pm 14)$ and $(\Phi, \psi) = (\pm 62, \pm 20)$ with an $rT = 18$. Regarding the loadings present in the structure, uniformly distributed potentials of 25 V were considered for each piezoelectric layer and the finite element discretization considered is (20×20) elements. In Figure 3, the reference system and the lamination schemes are presented. Furthermore, Figure 4 illustrates a schematic representation of the MBCs in a typical plate.

The results show that there are no significant differences in the mechanical response between the QUAD and DD laminates. This behavior arises because the DD laminate is equivalent to the QUAD laminate considering the identical membrane stiffness matrix ($[A]^*$) or identical bending stiffness ($[D]^*$). However, the DD has a larger generalized stiffness than the QUAD, which translates into an increase in natural frequencies. The coefficients of variation show low variability for identical DD laminates in terms of bending stiffness and higher variability for laminates with identical membrane stiffness. In this context, the results for DD with identical membrane stiffness are more significant, producing, for example, higher fundamental frequencies in the dynamic scenario than QUAD and, in some cases, DD with identical bending stiffness. The influence of electromechanical coupling is additionally evident, with the open sensor mode having greater frequencies than the short-circuit mode.

The relationship between the behavior associated with the membrane stiffness matrix, bending stiffness, and the MBCs is an important point to emphasize. This phenomenon may be seen more clearly in the dynamic results, where the DD in $[A]^*$ had higher frequencies than the DD in $[D]^*$ and the QUAD for the SSSS, SSCC, and SSCS MBCs. The behavior on SSFF, SSFC, and CCFF MBCs is reversed, with greater frequencies for the DD in $[D]^*$ and for the QUAD. Therefore, the fundamental frequency can be arranged in the following order for the QUAD and DD-$[D]^*$ going from lowest to highest: SSFF < SSFC < SSSS < SSCS < CCFF < SSCC. For the DD-$[A]^*$, the following order applies: SSFF < SSFC < SSSS < CCFF < SSCS < SSCC. Tables 14 and 15 show samples of the static and dynamic results Figure 5, presents the actuating mode shapes under different MBCs.

3.2.2. Tapering of laminated structures

In this case, a static and dynamic analysis is made of hybrid laminated plates and beams with different tapering schemes.

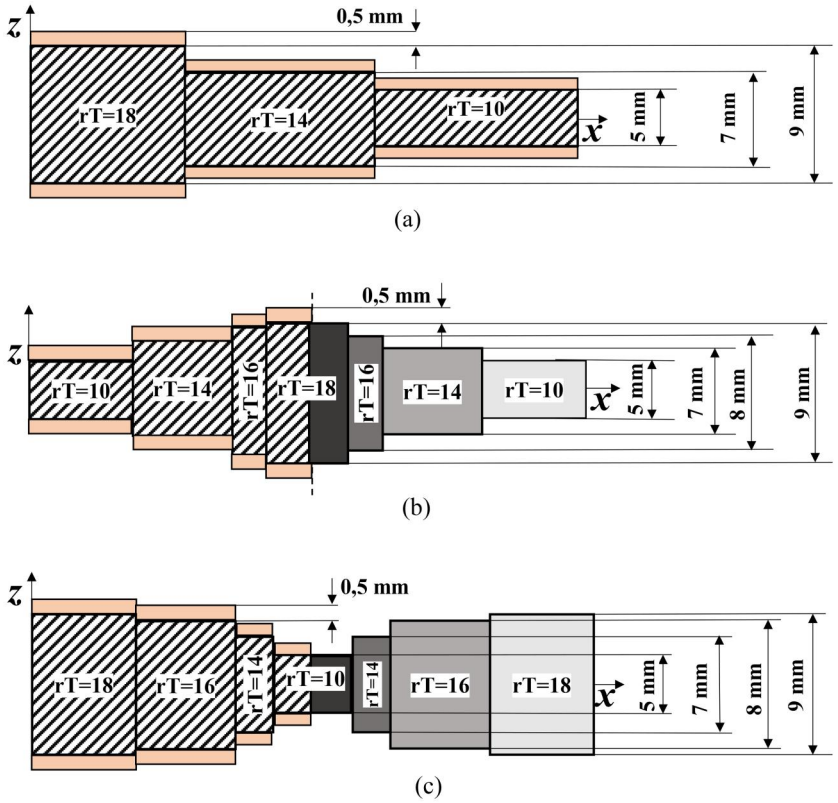

Figure 6. Schematic representation—side view (*xOz* plane) of the type of tapering: (a) tapering-1 (1D) of the beam; (b) tapering-2 (2D) of the plate; (c) tapering-3 (2D) of the plate.

Table 16. Static response of hybrid laminated beams considering the various lamination schemes of variable thickness (tapering-1) and constant, CFFF in actuator mode—sample results.

Static: Displacement w (μm) – Beam										
MBCs	Volt	Equiv	Tapering	[p/QUAD/p]	Stagg1	Stagg2	Stagg3	Stagg4	Paired1	Paired2
CFFF	25V	[*D*]*	Constant	13.816	13.881	13.896	13.899	13.911	13.899	13.896
CFFF	25V	[*D*]*	*Tapering-1*	–	19.545	19.575	19.582	19.609	19.581	19.578
CFFF	18V	[*D*]*	*Tapering-1*	–	14.073	14.094	14.099	14.118	14.098	14.096
CFFF	25V	[*A*]*	Constant	13.816	14.924	14.941	14.942	14.957	14.941	14.939
CFFF	25V	[*A*]*	*Tapering-1*	–	20.906	20.939	20.943	20.973	20.939	20.936

The tables utilize conditional formatting styles to vividly illustrate the results. Within the green-red color spectrum, lower values are represented by shades of green while higher values are depicted in red. This colour gradient is an attempt to offer a clear depiction of the progression of the relevant physical quantity.

Table 17. Dynamic response of hybrid laminated beams considering different lamination schemes of variable thickness (tapering-1) and constant thickness, CFFF—sample results.

Dynamics: Fundamental frequency, ω (Hz) – Beam, CFFF															
[p/QUAD/p]			Stagg1		Stagg2		Stagg3		Stagg4		Paired1		Paired2	
Eq	OC	CC	OC	CC	OC	CC	OC	CC	OC	CC	OC	CC	OC	CC
[*D*]*	118.371	117.857	118.116	117.607	118.114	117.604	118.057	117.547	118.056	117.545	118.076	117.566	118.077	117.566
[*D*]*	*Tapering-1*		124.526	123.944	124.524	123.940	124.449	123.866	124.447	123.863	124.475	123.891	124.475	123.892
[*A*]*	118.371	117.857	112.220	111.714	112.222	111.715	112.174	111.667	112.175	111.668	112.194	111.686	112.193	111.686
[*A*]*	*Tapering-1*		118.489	117.911	118.492	117.912	118.429	117.850	118.431	117.850	118.455	117.876	118.455	117.875

The tables utilize conditional formatting styles to vividly illustrate the results. Within the green-red color spectrum, lower values are represented by shades of green while higher values are depicted in red. This colour gradient is an attempt to offer a clear depiction of the progression of the relevant physical quantity.

The materials and QUAD and DD lamination schemes are the same as presented previously, with identical lateral dimensions for the plate and beams, $L = 0.3$ m, $b = 0.03$ m. The thicknesses of the structures vary along the length and width of the structure as shown in Figure 6. Regarding the loading present in the structure, uniformly distributed potentials of 25 V were considered for each piezoelectric layer in actuator mode and a UDL of 1000 Pa in the case of the sensor (open circuit). The discretization considered for the plate is (20 × 20) and (6 × 60) for the beam. The MBCs used are CFFF for the beams and SSSS for the plates.

The results show not just the benefit of generating a tendentially homogenized laminate, but also how easily the DD approach promotes tapering. The displacements between the

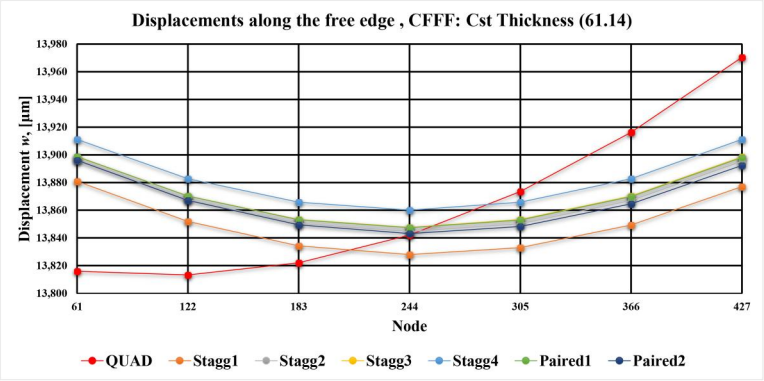

Figure 7. Graphical representation of the displacement profile along the free edge of CFFF beams, considering the various lamination schemes with constant thickness in actuator mode.

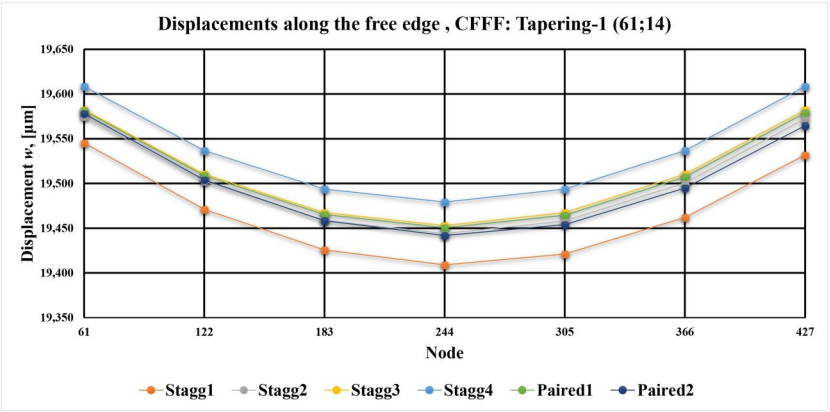

Figure 8. Graphical representation of the displacement profile along the free edge of CFFF beams, considering the various lamination schemes with tapered thickness in actuator mode.

Table 18. Static response of hybrid laminated plates considering the different lamination schemes of variable thickness (tapering-2 and tapering-3 in $[D]^*$) and constant, SSSS in actuator mode—sample results.

Static: Displacement at the center (μm) – Plate								
MBCs	Thickness	[p/QUAD/p]	Stagg1	Stagg2	Stagg3	Stagg4	Paired1	Paired2
SSSS	Constant	3.257	3.248	3.250	3.250	3.251	3.248	3.248
	Tapering-2	–	5.709	5.714	5.712	5.716	5.708	5.707
	Tapering-3	–	3.789	3.791	3.790	3.792	3.788	3.787

The tables utilize conditional formatting styles to vividly illustrate the results. Within the green-red color spectrum, lower values are represented by shades of green while higher values are depicted in red. This colour gradient is an attempt to offer a clear depiction of the progression of the relevant physical quantity.

QUAD and DD laminates agree as the displacements found for constant thickness structures are quite close. Tables 16 and 17, show that the DD-Stagg1 equivalent in $[D]^*$ dominates, obtaining the smallest displacements and higher fundamental frequencies. It should be noted that, in structures with constant thickness, the QUAD exhibits unbalanced bending behavior along the free edge opposite to the clamped side. This phenomenon contrasts with the behavior observed in any of the DDs possessing either constant or tapered thickness, as illustrated in Figures 7 and 8.

Structures that are properly tapered have several advantages that can be seen in the results obtained: (1) reduction in volume and weight (20.67% for tapering-1, 27.30% for tapering-2, and 8.2% for tapering-3); (2) optimization of actuation power or energy efficiency, i.e. higher displacements are obtained for the same applied electrical potential or are identical to the displacement of the uniform structure using a lower potential; (3) balanced bending behavior due to homogenization trend; (4) increase in the system's natural frequency due to the elimination of mass within regions characterized by higher degrees of freedom. The difference in the behavior of the equivalent DDs in $[D]^*$ and $[A]^*$ may be due to the interaction between the behavior associated with the membrane stiffness matrix, bending stiffness, and the respective MBCs.

The results obtained for the plate-type structures show similar results where the effect of the type of tapering carried out can be seen. Tables 18 and 19 show that tapering toward the edges (tapering-2) leads to an increase in displacement and a decrease in natural frequencies. However, as observed previously in the case of the CFFF beam, tapering toward the zone with the least restricted degrees of freedom, i.e. the center of the plate (tapering-3) leads to a displacement similar to that of the constant thickness

Table 19. Dynamic response of hybrid laminated plates considering different lamination schemes of variable thickness (tapering-2 and tapering-3 in [*D*]*) and constant thickness, SSSS—sample results.

Dynamics: Fundamental frequency, ω (Hz) – Plate, SSSS														
[p/QUAD/p]			Stagg1		Stagg2		Stagg3		Stagg4		Paired1		Paired2	
Thick	OC	CC	OC	CC	OC	CC	OC	CC	OC	CC	OC	CC	OC	CC
Cst	638.790	632.550	639.460	633.230	639.290	633.060	639.370	633.140	639.250	633.010	639.460	633.220	639.500	633.270
Tapering-2			473.391	466.727	473.189	466.519	473.280	466.612	473.129	466.456	473.382	466.717	473.432	466.769
Tapering-3			556.052	550.986	555.877	550.807	555.967	550.899	555.836	550.764	556.051	550.984	556.095	551.029

The tables utilize conditional formatting styles to vividly illustrate the results. Within the green-red color spectrum, lower values are represented by shades of green while higher values are depicted in red. This colour gradient is an attempt to offer a clear depiction of the progression of the relevant physical quantity.

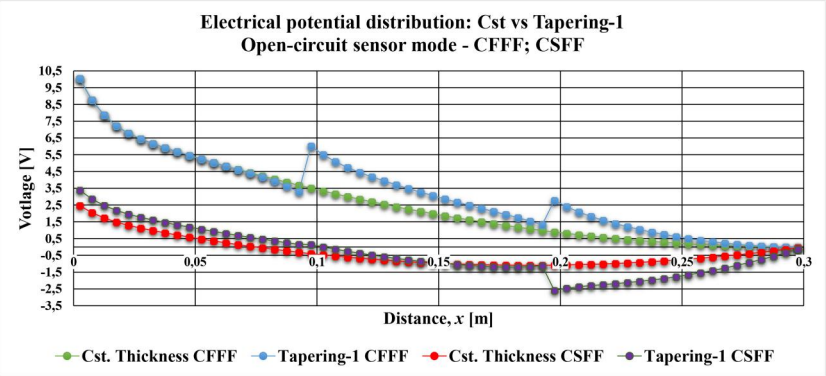

Figure 9. Graphical representation of the electrical potentials for a constant thickness beam with tapering-1 considering a UDL load for CFFF and CSFF.

structure for the same applied potential associating. A slight decrease in the fundamental frequency is also seen in this type of tapering as shown in Table 19.

Figure 9 shows the electrical potentials generated along the length of the beam according to its thickness. Its analysis reveals some discrepancies given the nature of the MBCs, the variation in thickness along the length of the structure, and the nature of the loading. While these outcomes are anticipated, they provide a means to confirm the possible increase in the potential generated by implementing scaling schemes in the case of UDL loads.

While DD laminates offer advantages when compared to conventional laminates, it is important to acknowledge some limitations. The achieving of full orthotropy and zero coupling in DD might require a higher ply count and that contradicts the goal of lightness. However, DD offers some advantages even with lower ply counts and, in many applications, achieving near-orthotropy and minimal coupling might be sufficient. Therefore, the DD approach can still provide good performance with fewer plies compared to conventional laminates. The contradiction in the goal of lightness is a valid concern and when weight is paramount, DD might not always be the ideal choice if one tries to replicate the behavior of a QUAD. According to Refs. [22], the full DD potential becomes accessible when one does not try to mimic conventional laminates but when the best combination of Φ, Ψ, and rT for a given set of loads is determined. Nevertheless, there are other options and as discussed in Ref. [31] by using QT stacks, it is possible to meet the homogeneity and uncoupling requirements with just a 7-ply stack and two different orientation angles, regardless of the orientation values. Moreover, general blending schemes as presented in Refs. [31,78] cannot be easily obtained by the DD approach.

4. Conclusions

The present work is concerned with the mechanical behavior of beam and plate hybrid composite structures constituted by fiber-reinforced DD laminates and piezoelectric materials. Diverse studies on their static and dynamic behavior were conducted under various boundary conditions and loadings.

The results of the hybrid laminates led to some novel solutions. The possibility of transforming QUAD into DD laminates exhibiting an equivalent behavior was verified, and it also demonstrated the simplicity gained in terms of ply stacking. In this context, a specificity regarding the behavior associated with the membrane stiffness matrix, bending stiffness, and mechanical boundary conditions imposed was observed.

It was possible to obtain laminates with tapered thicknesses in the presented structures, which is hard to achieve with the conventional QUAD approach, and the advantages observed in the actuation mode were as follows: (1) weight reduction (20.67% for tapering-1, 27.30% for tapering-2, and 8.2% for tapering-3); (2) optimization of the actuation power or energy efficiency, i.e. for a given applied electrical potential, greater displacements are achieved, or displacements identical to those of the uniform structure are attained using a lower potential; (3) balanced bending behavior due to homogenization trend; (4) increase in the fundamental frequency in the structure due to the removal of mass present in the zones with more free degrees of freedom. In sensor mode, the possibility of increasing the potential generated by implementing tapering schemes on the elastic core was shown. Finally, the presence of electromechanical coupling increases the stiffness of the structure, resulting in lower displacements for the static case and higher natural frequencies

for the dynamic case. Future assessments should include stress analysis across the structure and other related fields, such as the thermo-electro-magnetic-elastic fields. Following the observations made along the document, the implementation of a unified formulation, namely Carrera's Unified Formulation (CUF) and the use of quasi-trivial (QT) stacking sequences will be also important research lines to pursue.

Disclosure statement

No potential conflict of interest was reported by the author(s).

Funding

The authors acknowledge the support of FCT/MEC through Project IDMEC, LAETA UIDB/50022/2020.

ORCID

M. A. R. Loja http://orcid.org/0000-0002-4452-5840

References

[1] J.N. Reddy, On laminated composite plates with integrated sensors and actuators, Eng. Struct., vol. 21, no. 7, pp. 568–593, Jul. 1999. DOI: 10.1016/S0141-0296(97)00212-5.

[2] S. Kapuria, P. Kumari, and J.K. Nath, Efficient modelling of smart piezoelectric composite laminates: A review, Acta Mech., vol. 214, no. 1–2, pp. 31–48, 2010. DOI: 10.1007/s00707-010-0310-0.

[3] N. Sezer and M. Koç, A comprehensive review on the state-of-the-art of piezoelectric energy harvesting, Nano Energy, vol. 80, pp. 105567, 2020. DOI: 10.1016/j.nanoen.2020.105567.

[4] K.Y. Lam, X.Q. Peng, G.R. Liu, and J.N. Reddy, A finite-element model for piezoelectric composite laminates, Smart Mater. Struct., vol. 6, no. 5, pp. 583–591, 1997. DOI: 10.1088/0964-1726/6/5/009.

[5] M. Smith and S. Kar-Narayan, Piezoelectric polymers: Theory, challenges and opportunities, Int. Mater. Rev., vol. 67, no. 1, pp. 65–88, 2022. DOI: 10.1080/09506608.2021.1915935.

[6] S.Q. Zhang, G.Z. Zhao, M.N. Rao, R. Schmidt, and Y.J. Yu, A review on modeling techniques of piezoelectric integrated plates and shells, J. Intell. Mater. Syst. Struct., vol. 30, no. 8, pp. 1133–1147, May 2019. DOI: 10.1177/1045389X19836169.

[7] M. Safaei, H.A. Sodano, and S.R. Anton, A review of energy harvesting using piezoelectric materials: state-of-the-art a decade later (2008–2018), Smart Mater. Struct., vol. 28, no. 11, pp. 113001, 2019. DOI: 10.1088/1361-665X/ab36e4.

[8] A. Aabid, B. Parveez, A. Raheman, Y.E. Ibrahim, A. Anjum, M. Hrairi, N. Parveen, and J.M. Zayan, A review of piezoelectric material-based structural control and health monitoring techniques for engineering structures: Challenges and opportunities, Actuators, vol. 10, no. 5, pp. 101, May 2021. DOI: 10.3390/act10050101.

[9] F. Kpeky, F. Abed-Meraim, H. Boudaoud, and E.M. Daya, Linear and quadratic solid–shell finite elements SHB8PSE and SHB20E for the modeling of piezoelectric sandwich structures, Mech. Adv. Mater. Struct., vol. 25, no. 7, pp. 559–578, May 2018. DOI: 10.1080/15376494.2017.1285466.

[10] D.A. Saravanos and P.R. Heyliger, Mechanics and computational models for laminated piezoelectric beams, plates, and shells, Appl. Mech. Rev., vol. 52, no. 10, pp. 305–320, Oct. 1999. DOI: 10.1115/1.3098918.

[11] A. Benjeddou, Advances in piezoelectric finite element modeling of adaptive structural elements: A survey, Comput. Struct., vol. 76, no. 1–3, pp. 347–363, 2000. DOI: 10.1016/S0045-7949(99)00151-0.

[12] E. Carrera, Historical review of Zig-Zag theories for multilayered plates and shells, Appl. Mech. Rev., vol. 56, no. 3, pp. 287–308, May 2003. DOI: 10.1115/1.1557614.

[13] E. Carrera, I. Elishakoff, and M. Petrolo, Who needs refined structural theories? Compos. Struct., vol. 264, pp. 113671, Jan. 2021. DOI: 10.1016/j.compstruct.2021.113671.

[14] N. Chattaraj and R. Ganguli, Performance improvement of a piezoelectric bimorph actuator by tailoring geometry, Mech. Adv. Mater. Struct., vol. 25, no. 10, pp. 829–835, 2017. DOI: 10.1080/15376494.2017.1308590.

[15] S.S. Raju, M. Umapathy, and G. Uma, Design and analysis of high output piezoelectric energy harvester using non-uniform beam, Mech. Adv. Mater. Struct., vol. 27, no. 3, pp. 218–227, 2018. DOI: 10.1080/15376494.2018.1472341.

[16] P.M. Anilkumar, A. Haldar, E. Jansen, B.N. Rao, and R. Rolfes, Design optimization of multistable variable-stiffness laminates, Mech. Adv. Mater. Struct., vol. 26, no. 1, pp. 48–55, 2019. DOI: 10.1080/15376494.2018.1512022.

[17] P. Kurt, B. Narayan, J.I. Roscow, and S. Orhan, Improving piezoelectric energy harvesting performance through mechanical stiffness matching, Mech. Adv. Mater. Struct., pp. 1–14, 2023. DOI: 10.1080/15376494.2023.2295383.

[18] E. Carrera, S. Brischetto, and P. Nali, Plates and Shells for Smart Structures Plates and Shells for Smart Structures: Classical and Advanced Theories for Modeling and Analysis, 1st ed. John Wiley & Sons Ltd, The Atrium, Southern Gate, Chichester, West Sussex, PO19 8SQ, United Kingdom, 2011.

[19] B. Vermes, S.W. Tsai, T. Massard, G.S. Springer, and T. Czigany, Design of laminates by a novel 'double–double' layup, Thin-Walled Struct., vol. 165, pp. 107954, 2021. DOI: 10.1016/j.tws.2021.107954.

[20] S.W. Tsai, Double–double: New family of composite laminates, AIAA J., vol. 59, no. 11, pp. 4293–4305, 2021. DOI: 10.2514/1.J060659.

[21] B. Vermes, S.W. Tsai, A. Riccio, F. Di Caprio, and S. Roy, Application of the Tsai's modulus and Double-Double concepts to the definition of a new affordable design approach for composite laminates, Compos. Struct., vol. 259, pp. 113246, 2020. DOI: 10.1016/j.compstruct.2020.113246.

[22] E. Kappel, Double–Double laminates for aerospace applications—Finding best laminates for given load sets, Compos. Part C Open Access., vol. 8, pp. 100244, Jul. 2022. DOI: 10.1016/j.jcomc.2022.100244.

[23] P. Vannucci, A new general approach for optimizing the performances of smart laminates, Mech. Adv. Mater. Struct., vol. 18, no. 7, pp. 548–558, 2011. DOI: 10.1080/15376494.2011.605015.

[24] A. Vincenti, P. Vannucci, and M.R. Ahmadian, Optimization of laminated composites by using genetic algorithm and the polar description of plane anisotropy, Mech. Adv. Mater. Struct., vol. 20, no. 3, pp. 242–255, 2013. DOI: 10.1080/15376494.2011.563415.

[25] M. Montemurro and A. Catapano, A new paradigm for the optimum design of variable angle tow laminates. In: A. Frediani, B. Mohammadi, O. Pironneau, and V. Cipolla, ed., Variational Analysis and Aerospace Engineering, Springer Optimization and Its Applications, vol. 116, Springer International Publishing, Cham, pp. 375–400, 2016.

[26] M. Montemurro, M.I. Izzi, J. El-Yagoubi, and D. Fanteria, Least-weight composite plates with unconventional stacking sequences: Design, analysis and experiments, J. Compos. Mater., vol. 53, no. 16, pp. 2209–2227, 2019. DOI: 10.1177/0021998318824783.

[27] A. Catapano and M. Montemurro, Strength optimisation of variable angle-tow composites through a laminate-level failure

criterion, J. Optim. Theory Appl., vol. 187, no. 3, pp. 683–706, 2020. DOI: 10.1007/s10957-020-01750-6.
[28] M.P. Scardaoni, M. Montemurro, E. Panettieri, and A. Catapano, New blending constraints and a stack-recovery strategy for the multi-scale design of composite laminates, Struct. Multidisc. Optim., vol. 63, no. 2, pp. 741–766, 2021. DOI: 10.1007/s00158-020-02725-x.
[29] Y. Wang, D. Wang, Y. Zhong, D.W. Rosen, S. Li, and S.W. Tsai, Topology optimization of Double-Double (DD) composite laminates considering stress control, Comput. Methods Appl. Mech. Eng., vol. 414, pp. 116191, 2023. DOI: 10.1016/j.cma.2023.116191.
[30] T. Garulli, A. Catapano, M. Montemurro, J. Jumel, and D. Fanteria, Quasi-trivial stacking sequences for the design of thick laminates, Compos. Struct., vol. 200, no. 15, pp. 614–623, 2018. DOI: 10.1016/j.compstruct.2018.05.120.
[31] M.P. Scardaoni and M. Montemurro, The design of blended laminates regardless of the stack: the search propagation direction, Compos. Commun., vol. 36, pp. 101385, 2022. DOI: 10.1016/j.coco.2022.101385.
[32] S.W. Tsai and J.D.D. Melo, An invariant-based theory of composites, Compos. Sci. Technol., vol. 100, pp. 237–243, 2014. DOI: 10.1016/j.compscitech.2014.06.017.
[33] G. Verchery, Les Invariants des Tenseurs d'Ordre 4 du Type de l'Élasticité. In: J.P. Boehler, ed., Mechanical Behavior of Anisotropic Solids/Comportment Méchanique Des Solides Anisotropes, Springer, Dordrecht, 1982.
[34] P. Vannucci and G. Verchery, A special class of uncoupled and quasi-homogeneous laminates, Compos. Sci. Technol., vol. 61, no. 10, pp. 1465–1473, 2001. DOI: 10.1016/S0266-3538(01)00039-2.
[35] P. Vannucci, Anisotropic Elasticity, Lecture Notes in Applied and Computational Mechanics, Springer Singapore, Singapore, 2019.
[36] M. Montemurro, The polar analysis of the third-order shear deformation theory of laminates, Compos. Struct., vol. 131, pp. 775–789, 2015. DOI: 10.1016/j.compstruct.2015.06.016.
[37] S.W. Tsai, A. Arteiro, and J.D.D. Melo, A trace-based approach to design for manufacturing of composite laminates, J. Reinf. Plast. Compos., vol. 35, no. 7, pp. 589–600, 2016. DOI: 10.1177/0731684415624770.
[38] S.W. Tsai, S. Sihn, and J.D.D. Melo, Trace-based stiffness for a universal design of carbon-fiber reinforced composite structures, Compos. Sci. Technol., vol. 118, pp. 23–30, 2015. DOI: 10.1016/j.compscitech.2015.08.003.
[39] J.D.D. Melo, J. Bi, and S.W. Tsai, A novel invariant-based design approach to carbon fiber reinforced laminates, Compos. Struct., vol. 159, pp. 44–52, 2017. DOI: 10.1016/j.compstruct.2016.09.055.
[40] S.W. Tsai and J.D.D. Melo, A unit circle failure criterion for carbon fiber reinforced polymer composites, Compos. Sci. Technol., vol. 123, pp. 71–78, 2016. DOI: 10.1016/j.compscitech.2015.12.011.
[41] S.K. Ha and C.A. Cimini, Theory and validation of the master ply concept for invariant-based stiffness of composites, J. Compos. Mater., vol. 52, no. 12, pp. 1699–1708, 2018. DOI: 10.1177/0021998317728782.
[42] R.M. Guedes, Validation of trace-based approach to elastic properties of multidirectional glass fibre reinforced composites, Compos. Struct., vol. 257, pp. 113170, Feb. 2021. DOI: 10.1016/j.compstruct.2020.113170.
[43] A. Arteiro, L.F. Pereira, M.A. Bessa, C. Furtado, and P.P. Camanho, A micro-mechanics perspective to the invariant-based approach to stiffness, Compos. Sci. Technol., vol. 176, pp. 72–80, 2019. DOI: 10.1016/j.compscitech.2019.04.002.
[44] A. Arteiro, N. Sharma, J.D.D. Melo, S.K. Ha, A. Miravete, Y. Miyano, T. Massard, P.D. Shah, S. Roy, R. Rainsberger, K. Rother, C. Cimini Jr., J.M. Seng, F.K. Arakaki, T.-E. Tay, W.I. Lee, S. Sihn, G.S. Springer, A. Roy, A. Riccio, and H.T. Hahn, A case for Tsai's Modulus, an invariant-based approach to stiffness, Compos. Struct., vol. 252, pp. 112683, 2020. DOI: 10.1016/j.compstruct.2020.112683.
[45] S.L.J. Millen, B.G. Falzon, and M.A. Aravand, Invariant based approaches in the design of composite laminates, Compos. Sci. Technol., vol. 202, pp. 108526, Jan. 2021. DOI: 10.1016/j.compscitech.2020.108526.
[46] L.L. Vignoli, R.M.C. Neto, M.A. Savi, P.M.C.L. Pacheco, and A.L. Kalamkarov, Trace theory applied to composite analysis: A comparison with micromechanical models, Compos. Commun., vol. 25, pp. 100715, 2021. DOI: 10.1016/j.coco.2021.
[47] L. Jia, C. Zhang, J. Li, L. Yao, and C. Tang, Validation and development of trace-based approach for composite laminates, Compos. Sci. Technol., vol. 221, pp. 109348, 2022. DOI: 10.1016/j.compscitech.2022.109348.
[48] L.L. Vignoli, Is the out-of-plane shear strength an independent property? A micromechanical perspective about a macromechanical question, J. Compos. Mater., vol. 57, no. 28, pp. 4379–4388, 2023. DOI: 10.1177/00219983231209488.
[49] R.M. Patel and C.K. Desai, Master ply concept using invariant-based design approach for fused deposition modeling material, J. Inst. Eng. India. Ser. C., vol. 104, no. 4, pp. 789–796, Aug. 2023. DOI: 10.1007/s40032-023-00958-5.
[50] S.W. Tsai and J.D.D. Melo, Composite Materials Design and Testing Unlocking Mystery with Invariants, Composites Design Group Department of Aeronautics & Astronautics Stanford University, Stanford, CA 94305-4035, 2015.
[51] S.W. Tsai, J.D.D. Melo, S. Sihn, A. Arteiro, and R. Rainsberger, Composite Laminates: Theory and Practice of Analysis, Design and Automated Layup. Composites Design Group Department of Aeronautics & Astronautics Stanford University, Stanford, CA 94305-4035, 2017.
[52] S.W. Tsai, N. Sharma, A. Arteiro, S. Roy, and B. Rainsberger, Composite Double-Double and Grid/Skin Structures – Low Weight/Low Cost Design and Manufacturing, Stanford University; Composites Design Group, Stanford, CA, 2019.
[53] S.W. Tsai, Double-Double: A New Perspective in the Manufacture and Design of Composites, Stanford University; Composites Design Group, Stanford, CA, 2022.
[54] Z. Zhang, Z. Zhang, F. Di Caprio, and G.X. Gu, Machine learning for accelerating the design process of Double-Double composite structures, Compos. Struct., vol. 285, pp. 115233, 2022. DOI: 10.1016/j.compstruct.2022.115233.
[55] A. Vescovini, C.X. Li, J. Paz Mendez, B.C. Jin, A. Manes, and C. Bisagni, Post-buckling behavior and collapse of Double-Double composite single stringer specimens, Compos. Struct., vol. 327, pp. 117699, 2023. DOI: 10.1016/j.compstruct.2023.117699.
[56] M.F.S.F. de Moura, A.B. de Morais, and A.G. de Magalhães, Materiais Compósitos – Materiais, Fabrico e Comportamento Mecânico, Publindústria, Edições Técnicas Praça da Corujeira n.° 38. 4300-144 PORTO, 2010. www.publindustria.pt
[57] J.D. Emery and C.P. Mentesana, Piezoelectric Theory for Finite Element Analysis of Ultrasonic Motors, Technical Report, Research Org.: AlliedSignal Federal Manufacturing and Technologies, Kansas City, MO, Jun. 1997. DOI: 10.2172/650248.
[58] S.Y. Wang, A finite element model for the static and dynamic analysis of a piezoelectric bimorph, Int. J. Solids Struct., vol. 41, no. 15, pp. 4075–4096, Jul. 2004. DOI: 10.1016/j.ijsolstr.2004.02.058.
[59] R. Ogden, and D. Steigmann, Mechanics and Electrodynamics of Magneto- and Electro-Elastic Materials, vol. 527, Springer Vienna, Vienna, 2011. DOI: 10.1007/978-3-7091-0701-0.
[60] C.K. Lee, Theory of laminated piezoelectric plates for the design of distributed sensors/actuators. Part I: Governing equations and reciprocal relationships, J. Acoust. Soc. Am., vol. 87, no. 3, pp. 1144–1158, 1990. DOI: 10.1121/1.398788.
[61] V.M. Franco Correia, M.A. Aguiar Gomes, A. Suleman, C.M. Mota Soares, and C.A. Mota Soares, Modelling and design of adaptive composite structures, Comput. Methods Appl. Mech.

Eng., vol. 185, no. 2–4, pp. 325–346, 2000. DOI: 10.1016/S0045-7825(99)00265-0.

[62] J.N. Reddy, Mechanics of Laminated Composite Plates and Shells, 2nd ed. Boca Raton CRC Press LLC, 2000 N.W. Corporate Blvd., Boca Raton, Florida 33431, 2003. DOI: 10.1201/b12409.

[63] M.A. Ramos Loja, C.M. Mota Soares, and C.A. Mota Soares, Modelling and design of adaptive structures using B-spline strip models, Compos. Struct., vol. 57, no. 1–4, pp. 245–251, Jul. 2002. DOI: 10.1016/S0263-8223(02)00091-0.

[64] M.A.R. Loja, J. Infante Barbosa, C.M. Mota Soares, and C.A. Mota Soares, Analysis of piezolaminated plates by the spline finite strip method, Comput. Struct., vol. 79, no. 26–28, pp. 2321–2333, Nov. 2001. DOI: 10.1016/S0045-7949(01)00065-7.

[65] C.M. Mota Soares, C.A. Mota Soares, V.M. Franco Correia, and M.A. Ramos Loja, Higher-order B-spline strip models for laminated composite structures with integrated sensors and actuators, Compos. Struct., vol. 54, no. 2–3, pp. 267–274, 2001. DOI: 10.1016/S0263-8223(01)00097-6.

[66] S.W. Tsai, J.D.D. Melo, S. Sihn, A. Arteiro, and R. Rainsberger, Composite Laminates: Theory and Practice of Analysis, Design and Automated Layup, Stanford University; Composites Design Group, Stanford, CA, 2017.

[67] E. Carrera, Theories and finite elements for multilayered plates and shells: A unified compact formulation with numerical assessment and benchmarking, ARCO, vol. 10, no. 3, pp. 215–296, 2003. DOI: 10.1007/BF02736224.

[68] A. Robaldo, E. Carrera, and A. Benjeddou, A unified formulation for finite element analysis of piezoelectric adaptive plates, Comput. Struct., vol. 84, no. 22–23, pp. 1494–1505, 2006. DOI: 10.1016/j.compstruc.2006.01.029.

[69] D. Ballhause, M. D'Ottavio, B. Kröplin, and E. Carrera, A unified formulation to assess multilayered theories for piezoelectric plates, Comput. Struct., vol. 83, no. 15–16, pp. 1217–1235, 2005. DOI: 10.1016/j.compstruc.2004.09.015.

[70] E. Carrera and A. Ciuffreda, A unified formulation to assess theories of multilayered plates for various bending problems, Compos. Struct., vol. 69, no. 3, pp. 271–293, 2005. DOI: 10.1016/j.compstruct.2004.07.003.

[71] G.H. Altenbach and E. Carrera, Kulikov, Analysis and Modelling of Advanced Structures and Smart Systems, Springer Singapore. 152 Beach Road, #21-01/04 Gateway East, Singapore 189721, Singapore, vol. 81, 2018.

[72] A.J.M. Ferreira, A.L. Araújo, A.M.A. Neves, J.D. Rodrigues, E. Carrera, M. Cinefra, and C.M.M. Soares, A finite element model using a unified formulation for the analysis of viscoelastic sandwich laminates, Compos. Part B Eng., vol. 45, no. 1, pp. 1258–1264, Feb. 2013. DOI: 10.1016/j.compositesb.2012.05.012.

[73] P. Heyliger and D.A. Saravanos, Exact free-vibration piezoelectric layers, J. Acoust. Soc. Am., vol. 98, no. 3, pp. 1547–1557, 2014. DOI: 10.1121/1.413420.

[74] A. Benjeddou and J.-F. Deü, A two-dimensional closed-form solution for the free-vibrations analysis of piezoelectric sandwich plates, Int. J. Solids Struct., vol. 39, no. 6, pp. 1463–1486, Mar. 2002. DOI: 10.1016/S0020-7683(01)00287-6.

[75] A.A. Khdeir, Comparison between shear deformable and Kirchhoff theories for bending, buckling and vibration of antisymmetric angle-ply laminated plates, Compos. Struct., vol. 13, no. 3, pp. 159–172, Jan. 1989. DOI: 10.1016/0263-8223(89)90001-9.

[76] S. Cen, A.-K. Soh, Y.-Q. Long, and Z.-H. Yao, A new 4-node quadrilateral FE model with variable electrical degrees of freedom for the analysis of piezoelectric laminated composite plates, Compos. Struct., vol. 58, no. 4, pp. 583–599, 2002. DOI: 10.1016/S0263-8223(02)00167-8.

[77] D.A. Saravanos, P.R. Heyliger, and D.A. Hopkins, Layerwise mechanics and finite element for the dynamic analysis of piezoelectric composite plates, Int. J. Solids Struct., vol. 34, no. 3, pp. 359–378, Jan. 1997. DOI: 10.1016/S0020-7683(96)00012-1.

[78] M. Picchi Scardaoni, M.I. Izzi, M. Montemurro, E. Panettieri, V. Cipolla, and V. Binante, Multi-scale deterministic optimisation of blended composite structures: Case study of a box-wing, Thin-Walled Struct., vol. 170, pp. 108521, 2021. DOI: 10.1016/j.tws.2021.108521.